Discovering Solar Materials Through Materials Modeling

A Major Qualifying Project
Submitted to the Faculty of
Worcester Polytechnic Institute
in partial fulfillment of the requirements for the
Degree in Bachelor of Science
in
Chemical Engineering

By

Julia Bryant

Ashli Silvera

Hunter Wieckowski

Advised by
Professor N. Aaron Deskins

With Assistance from
Emily Sutherland (Physics Ph.D. Student)

1.0 Introduction

MXenes are 2D materials with the formula $M_{n+1}X_nT_x$—where M represents an early d-block transition metal, X represents a Carbon or Nitrogen atom, and T represents the surface terminations group—that have the potential for photocatalytic applications. Photocatalysis is the process in which a photocatalyst absorbs light, creating an electron-hole pair which creates an environment for oxidation, as the excited electrons are used to reduce an acceptor and the hole is used for the oxidation of donor molecules. MXenes can be useful in many applications because they are so customizable, as the M layer can be a variety of early transition metals and the termination group can be changed to be F, O, OH, etc. For instance, by changing the termination groups on a MXene, the alignment of electronic states can be adjusted. In photocatalysis, MXenes are mainly useful for promoting photogenerated charge carrier separation due to their Fermi level which is lower than most known semiconductors and therefore allows electrons to flow from the semiconductor to the MXene. MXenes properties can be simulated using density functional theory (DFT) calculations to reduce the need for laboratory testing.

In this report, we discuss the role of MXenes in photocatalysis and how DFT can be used to model MXenes. We then present our methodology for calculating MXene properties—lattice parameter, magnetic moment, density of states, band structure, work function—using VASP and provide an analysis of our results. Finally, based on our calculations, we recommend that $Cr_3C_2F_2$ may be useful for photocatalysis due to its high density of states and work function higher than that of Si:H, a common semiconductor used in solar panels. $V_3C_2O_2$ may also be useful, although it does not have an especially high density of states. $Sc_3C_2F_2$ was the only MXene modeled to exhibit semiconductor properties, so this MXene could also be useful but further analysis and calculation of more properties is recommended.

2.0 Background

2.1 What are MXenes?

MXenes, pronounced "maxenes," are a relatively new class of 2D materials that were discovered in 2011 and have garnered the attention of many working in the field of material science. This is due to the set of attractive properties MXenes have that make them suitable for many practical applications; these include but are not limited to their high conductivity, excellent photoelectric and electrochemical properties, and highly functional surface area (Champagne 2020). Figure 1 shows the structure of one MXene, $Ti_3C_2O_2$, with 1A displaying a 2-dimensional side view and 1B showing a 3-dimensional sheet.

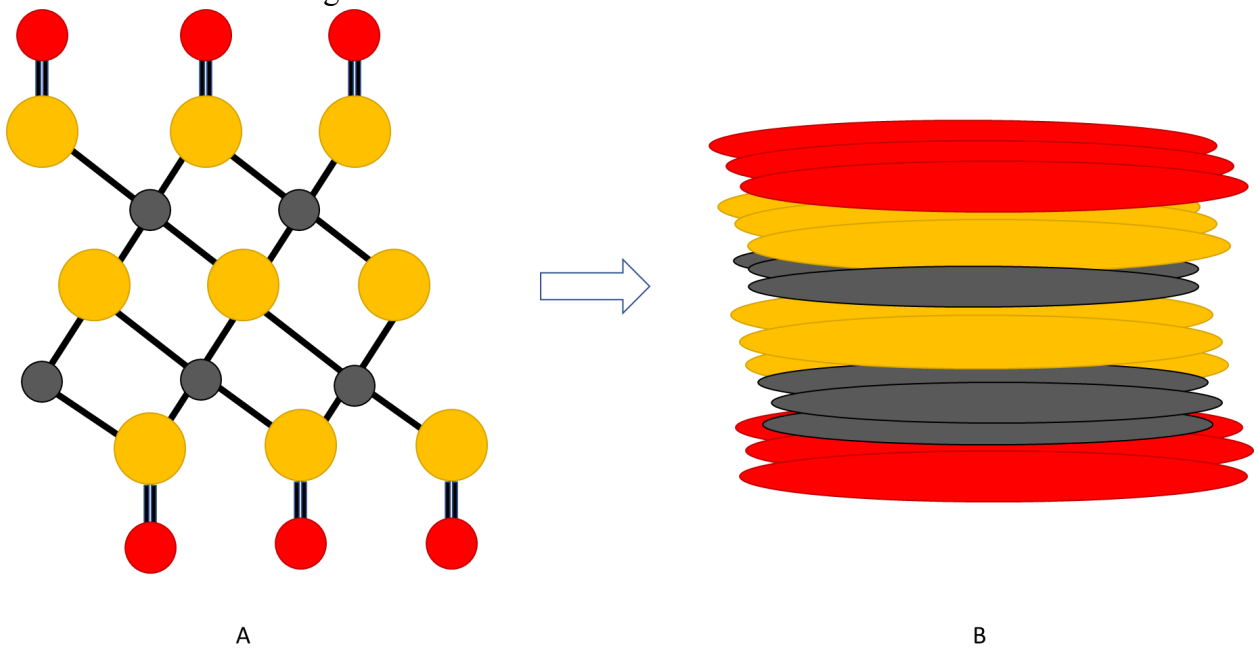

Figure 1: Structure of a MXene, $Ti_3C_2O_2$. (A): Side View of a MXene showing individual atoms. (B): Side view of a MXene showing the different layers that make up the 'sheet'.

Research into MXenes and 2D materials as a whole was brought on by the discovery of single-sheet graphene in 2004 (Gogotsi, 2021). Single sheet graphene is composed of one layer of carbon atoms that are sp^2 bonded in a hexagonal orientation. It has superior electrical and mechanical properties compared to that of its 3D graphite precursor. Because of this phenomenon, there has been a large recent interest in the 2D analogs of other 3D materials, with the goal being to find more 2D materials with exceptional properties. This has led to the discovery of many new families of 2D materials in the years since. MXenes are one of these new materials, and they have many potential applications, while still requiring more research to be done to fully characterize and commercialize them.

MXenes refer to a class of materials that all share a similar structure, which is related to their name. All MXenes follow the general formula $M_{n+1}X_nT_x$, where M represents an early d-block transition metal, X represents a Carbon or Nitrogen atom, and T represents the surface terminations group which is generally O, OH, F, or Cl (Shuck, 2020) The surface terminations are bonded to outer M layers when the MXene is derived from its precursor 3D MAX phase. These MAX phases are layered ternary carbides or nitrides. The A in these MAX phases represents main-group sp elements, most commonly those belonging to the IIIA or IVA group.

MXenes can be synthesized by selectively etching the A atoms of a MAX phase with an acid mixture. This etching process exposes the M atoms to the acid mixture and, depending on the mixture, determines what function groups randomly distribute along the surface (Caffrey, 2018). The first single layer MXene that was successfully synthesized, $Ti_3C_2T_x$, was produced in 2013 by etching Ti_3AlC_2 with hydrofluoric acid. Other etchants such as HCl and LiF have also been used to synthesize MXenes (Gogotsi, 2019). Etching time is another factor that can impact a MXene's structure (Cui, 2019). The etchants and method used to synthesize MXenes can vary based on the desired surface terminations, but in general, a Lewis acidic melt etching method is preferred. This is a top-down approach method in which a molten salt, such as $ZnCl_2$, acts as a Lewis acid and thermodynamically reacts with the A element of a MAX phase, stripping it from the remaining composite. This method is generally more preferred as it does not require the use of HF, making it a safer and cleaner method (Li, M, 2019). There have been many more MXenes successfully synthesized since 2013. Some of these include: Ti_2C, Ti_3C_2, Nb_2C, Ti_3CN, Ta_4C_3, V_2C, and Nb_4C_3 (Li, X, 2018). Several new subfamilies of MXenes have also been discovered, such as the ordered double-transition metal MXenes which follow the formula, $M'_2M''C_2$ or $M'_2M''_2C_3$, where M' and M'' are two unique transition metals (Alhabeb, 2017). The field of MXenes is quickly growing, and as of 2020, over 30 unique MXenes have been successfully synthesized, and even more have been modeled using computational methods (Huang, 2020).

2.1.1 Properties of MXenes

The properties of MXenes are what make them noteworthy in the field of material science and especially in the area of 2D materials. Compared to other 2D materials, MXenes generally have a combination of high electrical conductivity, hydrophilic properties, and stability (Hart, 2019). The specific properties of each MXene are linked to its elemental composition and the surface termination groups present, so while generalizations can be made for the family of materials, individual MXenes do differ greatly from another (Zhan, 2020). When MXenes are synthesized the specific elements and etching material are chosen to produce a desired property (Alhabeb, 2017).

In general, the properties that make MXenes very desirable are their combination of high electrical and thermal conductivities, various magnetic ordering, and high Young's modulus (Champagne, 2020). The mechanical properties of MXenes are highly dependent on the surface termination groups present. For instance, it has been shown that MXenes with O terminated surface groups have a higher stiffness than the same MXenes with F and OH surface terminations (Zhan, 2020). This is due to the smaller lattice parameter of the O terminated MXenes. The number of atomic layers—denoted by n in the MXene chemical formula—also has been shown to have a large impact on the mechanical properties. MXenes with lower values of n have been found to have higher strength and hardness values. Due to their inherent 2D nature, MXenes have a large surface area to volume ratio, which is very useful for many of their applications.

The electronic properties of MXenes are especially important as they pertain to many of their common applications. 2D materials as a whole generally have extraordinary photoelectric and electrochemical properties, as well as a high electric conductivity due to their inherent physical shape (Kuang et al., 2020). Most MXenes are metallic, however, specific MXenes such as Ti_2CO_2, Zr_2CO_2, and Hf_2CO_2 have semiconducting properties due to their surface terminations (Khazaei, 2017). Whether a MXene has the electrical properties of being a metal or semiconductor is dependent on the chemical composition of the MXene itself, meaning an appropriate MAX phase and etchant must be selected to synthesize them. MXenes that are

semiconductors all have an indirect bandgap, except for $Sc_2C(OH)_2$, which has a direct bandgap (Champagne, 2020). Having the properties of a semiconductor allows these certain MXenes to perform as photocatalysts.

Semiconducting MXenes have other properties that make them suitable as photocatalysts. The surface termination groups O and OH give MXenes hydrophilic functionalities on their surfaces, which allow for strong interactions with water molecules (Li, X, 2018). The previously mentioned high conductivity is also desirable for photocatalysis, as it allows for high levels of electron mobility. The terminal metal sites, M group, exposed on MXenes allow for strong redox properties. MXenes also can have stability in aqueous solutions such as water. Not all MXenes are suited to act as photocatalysts, those that are can be synthesized specifically for the aforementioned properties.

2.1.2 Applications of MXenes

The attractive physical and electrical properties of MXenes allow them to have a wide variety of applications. Some MXenes are being considered as materials to use for sensors, specifically sensing pressure, strain, biochemicals, temperature, and gas. 2D materials have been being used in sensors for over a decade, as their large specific surface area and excellent conductive properties allow them to perform well in this role (Zhan, 2020). One reason why MXenes specifically make good sensors is that it is easy for MXenes to form composites with other materials, allowing for further property tuning. MXene composites show enhanced mechanical flexibility and stretchability enabling a wide application in the field of sensors (Xin, 2020). The majority of MXene applications, however, are related to energy in some way. MXenes are being considered and tested as battery electrodes, energy storage materials, and catalysts. MXenes are being considered as the anodes of Lithium-Ion Battery alternatives, which utilize cheaper, more common materials. MXenes such as TiO_xN_y/C and $K_2Ti_4O_9$ have already been tested for this application and have shown to have excellent rate performances and ideal energy densities (Aslam, 2020). An added bonus to using MXenes as opposed to other battery materials— such as lithium—is that MXenes are much more environmentally friendly. MXenes are typically made out of more readily available elements such as Titanium, whereas lithium is much less common. Lithium batteries are also toxic to the environment when they contain heavy metals or are disposed of in large quantities (Aral 2008). This holds true for other energy-based applications, such as photocatalysts.

2.2 What is Photocatalysis?

As mentioned previously, MXenes have many possible applications, but they have been most widely studied in the areas of energy conversion and storage. The conversion from solar energy to chemical fuel is a significant alternative for solving the current energy shortage and environmental crisis. Fortunately, photocatalytic technology has the potential for obtaining sustainable, renewable, and clean chemical fuels. This technology is cost-effective, environmentally friendly, and convenient. However, the main challenge is finding materials with high activity and stability to support this energy conversion. MXenes are a suitable material for promoting photocatalysis because of their “flexible adjustability of elemental composition, regular layered structure, and excellent electrical conductivity” (Cheng et al., 2019).

The focus of this project is the application of MXenes in solar energy through their role as a component in photocatalysis. Photocatalysis is a phenomenon in which a substrate— the photocatalyst— is exposed to and absorbs light, as shown in figure 2. This absorbed light excites

the electrons to the conduction band, which creates a hole in the valence band. This creates an environment for oxidation and reduction on the surface of the substrate/photocatalyst, as these excited electrons are used to reduce an acceptor and the hole is used for the oxidation of donor molecules. Photocatalysts are all basically semiconductors (Ameta et al., 2018).

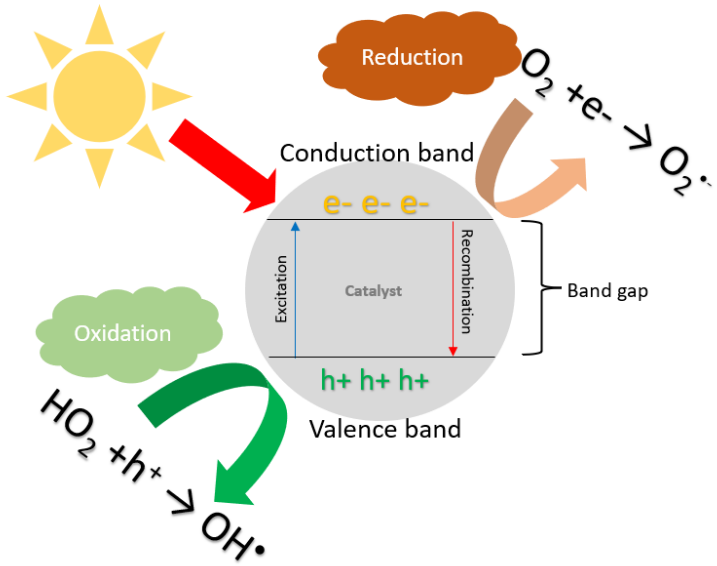

Figure 2: Illustrative diagram of the photocatalytic process. The photocatalyst, shown in gray, absorbs light from the sun which excites electrons (depicted by e- on the figure) to the conduction band, leaving holes (depicted as h+) in the valence band. This allows for reduction (shown in orange) of acceptors to occur using the excited electrons and oxidation (shown in green) of donor molecules using the holes.

The fate of the electron-hole pair is determined by two criteria: the position of bands of the semiconductor and the redox levels of the substrate. There are four possible processes that occur depending on these criteria, shown in figure 3. If the redox level of the substrate is lower than the conduction band of the semiconductor, reduction of the substrate occurs. When the redox level of the substrate is higher than the valence band of the semiconductor, oxidation occurs. Nothing occurs when the redox level of the substrate is higher than the conduction band and lower than the valence band of the semiconductor. Finally, both reduction and oxidation occur when the redox level of the substrate is lower than the conduction band and higher than the valence band (Ameta et al., 2018).

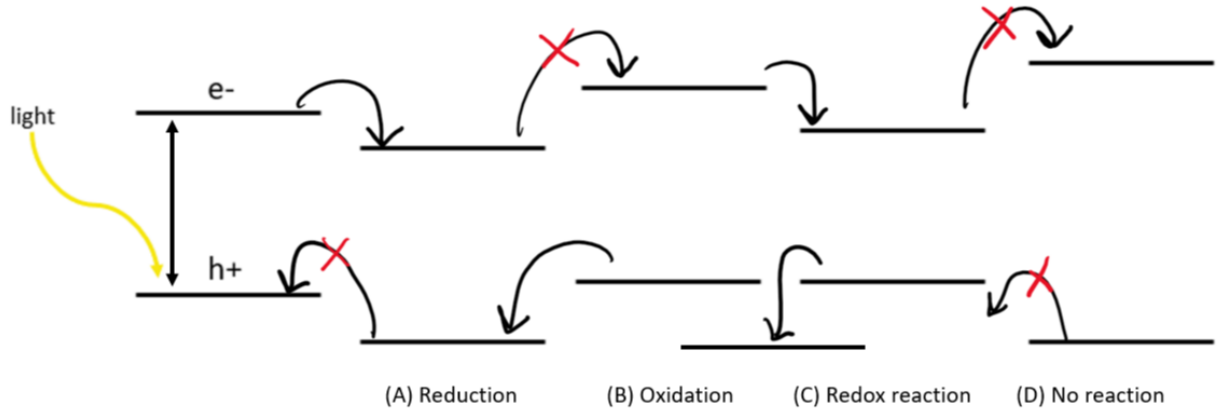

Figure 3: Four possible electron/hole transfer processes of the electron-hole pair from a semiconductor to a molecule. The leftmost energy levels are of the semiconductor photocatalyst and the energy levels for four possible molecules (indicated by four types of electron/hole transfer processes) are shown on the right.

The photocatalytic process is divided into three main steps. First is the generation of charge carriers—electrons and holes—upon exposure to light. Second is the separation and mitigation of charge carriers to the photocatalyst surface. This is the rate-determining step, as there is a slow transfer but a high recombination rate of electrons and holes (Ameta et al., 2018). Recombination refers to electrons jumping down from the conduction band to recombine with the holes generated in the valence band (Libretexts, 2021). MXenes, as will be discussed, come into play during this step, as their properties can help prevent recombination and therefore increase photocatalytic activity. The third and final step is the occurrence of redox reactions by consuming the electrons and holes.

2.2.1 Role of MXenes in Photocatalysis

As for the role of MXenes in photocatalysis, MXenes have the potential to enhance photocatalytic activity by serving as photo-generated electron acceptors, illustrated in figure 4 (Kuang et al., 2020). This is due to their Fermi level which is lower than most known semiconductors; when two materials are in contact, electrons will flow from the material with the higher Fermi level to the material with the lower Fermi level, which is the MXene in this case (Brittanica).

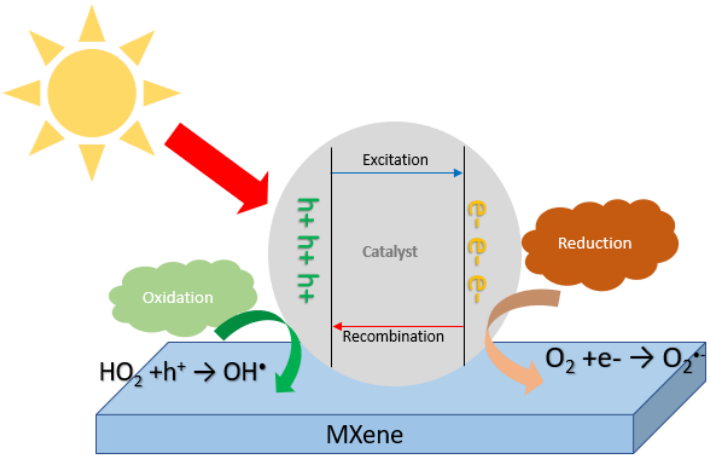

Figure 4: MXene-based photocatalysis, where the MXene surface serves as a photo-generated electron acceptor. When the MXene is in contact with the catalyst/semiconductor, electrons will flow from the catalyst to the MXene.

MXenes can be successful in photocatalysis for three main reasons. First, they have abundant functional groups which are beneficial for the construction of contact between MXenes and other semiconductors. Second, the bandgap alignment of MXenes can be altered by altering the surface chemistry of the MXene which can be useful. Thirdly, the conductive metal cores in the layered structure allow MXenes to have excellent metallic conductivity and electron acceptance ability (Kuang et al., 2020). However, MXenes alone have a narrow light absorption range and uncontrollable photocatalytic stability. Therefore, coupling MXenes with other photocatalysts helps improve their effectiveness (Cheng et al., 2019)

MXenes play a variety of roles in these photocatalytic applications, such as promoting photogenerated charge carrier separation, acting as robust support, limiting photocatalyst size, and enhancing reactant adsorption. Promoting charge carrier separation is essential in increasing photocatalytic activity. Modifying a photocatalyst with a cocatalyst to make a composite photocatalyst for separating the charge carriers is an effective way to do so. In composite photocatalysts, one component (the semiconductor) absorbs light, while the other components (the MXene) help separate the electrons and holes, or act as reaction centers (Figure 5).

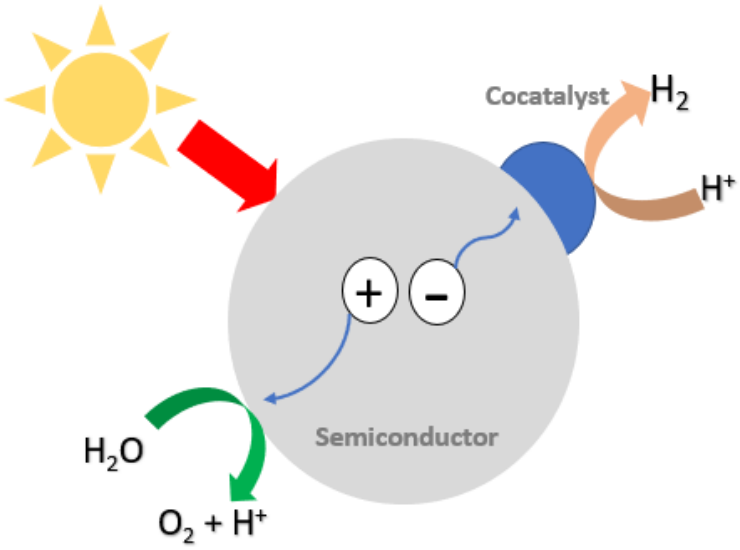

Figure 5: Semiconductor (photocatalyst) modified with a cocatalyst on its surface. In composite photocatalysts, the semiconductor absorbs light, while the cocatalyst (the MXene) helps separate the electrons and holes and can also act as reaction centers.

For example, the MXene Ti_3C_2 exhibits metallic conductivity with a Fermi level of -0.05 eV which is more positive than the conduction band of most n-type semiconductors. This suggests its potential as a cocatalyst for the transfer and accumulation of photogenerated electrons. A Schottky junction could be formed between Ti_3C_2 and CdS because electrons in the conduction band of CdS could migrate to Ti_3C_2 due to the lower fermi level of Ti_3C_2. Furthermore, the moderate H adsorption free energy of Ti_3C_2 means that H^+ can be reduced to H_2 (Kuang et al., 2020).

Another role MXenes can have in photocatalysis is to act as robust support for the growth of photocatalysts. The mechanical stability and large surface area of MXenes allow them to serve as support for uniform dispersion of photocatalysts, such as TiO_2, to expose surface-active sites for the reaction. MXenes' many surface functional groups are growing platforms for limiting the size of photocatalysts because aggregation into larger sizes decreases the contact area with the reactant. The negatively charged surface absorbs cations and allows for uniform growth (Kuang et al., 2020).

2.2.2 Applications of MXene-based Photocatalysis

The most studied applications of MXene-based photocatalysis are water splitting, CO_2 reduction, pollutant degradation, and N_2 fixation. Photocatalytic water splitting—the breakdown of water into H_2 and O_2—is considered the holy grail for energy supply, but its efficiency is not very high due to the recombination of electrons. MXenes, as mentioned prior, can help limit this recombination by guiding the flow of charge carriers onto semiconductors.

MXenes also have potential applications in CO_2 reduction. Photocatalysis could be used to convert CO_2 into carbon fuels and store solar energy in their chemical bond. Semiconductors studied for this application so far include TiO_2, CdS, and $ZnIn_2S_4$. MXenes are used to enhance the photocatalytic activity of these semiconductors. The fluffy structure formed when TiO_2 was grown on Ti_3C_2 sheets had a higher specific surface area than each compound alone, which provides more surface-active sites for photocatalysis (Kuang et al., 2020).

Photocatalysis has also shown potential in purifying water of organic pollutants. With its large surface area and excellent conductivity, TiO_2/Ti_3C_2 showed high photocatalytic activity for methyl orange degradation (Kuang et al., 2020). Ti_3C_2 could also improve the capability of Ag_2WO_4 in adorning antibiotic pollutants. Finally, there has been recent research on

solar-powered nitrogen fixation using Ti_3C_2, in which nitrogen could be adsorbed on Ti_3C_2. There is much more research needed in this area, but it provides another possible use for MXenes.

While there have been multiple new MXene discoveries, such as V_2C, Zr_2C, and Ti_2C, there is room for further research in photocatalytic applications of these MXenes. Research is also needed for more environmentally friendly ways to make MXenes and further development of strategies to determine the enhancement mechanism of MXenes in photocatalysis.

2.3 MXenes and DFT

Though there has been an explosion in the research of MXenes, there are many MXenes that have yet to be synthesized, so their exact properties are unknown. When researching MXenes, it is important to model them computationally, shown in figure 6, as it limits the time needed to be spent in the laboratory, as well as money spent on wasteful experimental arrangements of the material. There are many approaches to constructing a mathematical model. In this project, we will be focusing on a model designed using ab initio methods. Ab initio methods—also referred to as first-principles methods—are based on the laws of quantum mechanics. When using these methods to design models, only fundamental constants of physics are used as input parameters. These methods, therefore, provide a detailed way to determine the properties of materials without heavy reliance on experimental parameters.

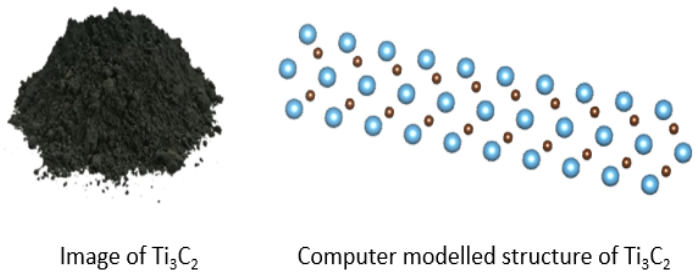

Figure 6: Side-by-side images of Ti_3C_2 MXene powder (left) (*Research Grade Titanium Carbide Two Dimensional MXene Ti3c2 Powder - Buy Ti3c2 Powder, MXene Titanium Carbide, MXene Ti3c2 Powder Product on Alibaba.com*) and the structure of Ti_3C_2 (right) visualized using VESTA software where the blue dots represent the Ti atoms and the brown dots represent C atoms.

2.3.1 Density Functional Theory

In modeling materials, it is important to understand how they behave at an atomic level, as the behavior exhibited at this level determines the properties of the material. Understanding materials at an atomic level, however, proves challenging as the laws of classical mechanics begin to break down. Therefore, an alternative theory is needed to account for the behavior of matter at the atomic level. This theory is quantum mechanics, and a description of the quantum behavior of atoms and molecules is provided by the Schrödinger equation [1] where $\widehat{H}$ represents the hamiltonian operator [2], and Ψ represents the wave function and E the energy of the system. This is an eigenproblem, where the energy E is the eigenvalue and the wave function is the eigenfunction.

$$\widehat{H}\Psi = E\Psi \quad [1]$$

$$\widehat{H} = \frac{-h^2}{m}\nabla^2 + V \quad [2]$$

Kinetic energy Potential energy

The Hamiltonian operator described above is only applicable to a single particle system. When expanded to account for the many-particle systems of materials we model, the Hamiltonian operator becomes much more complex. However, with the application of the Born-Oppenheimer Approximation, which treats the nucleus as a classical particle, the Hamiltonian is simplified, as shown in equation [3] (Sholl et al., 2011). Even with this simplification, the complete solution to the Schrödinger equation cannot be solved analytically. However, the density functional theory (DFT) model provides a relatively simple means of finding a numerical approximation to the Schrödinger equation.

$$\widehat{H} = -\frac{1}{2}\sum_{i=1}^{N}\nabla_i^2 - \sum_{i=1}^{N}\sum_{A=1}^{M}\frac{Z_A}{r_{iA}} + \sum_{i=1}^{N}\sum_{j>1}^{N}\frac{1}{r_{ij}} \quad [3]$$

Kinetic energy of electron electron-nucleus interaction electron-electron interaction

The DFT model is based on two mathematical theorems proven by Hohenberg and Kohn. The first theorem showed that the ground state from Schrödinger's equation is a unique functional of the electron density. In describing the quantum behavior of atoms, it is important to define their positions. The position of an atom can be broken down into the position of the nucleus of the atom and the position of the electrons in the atom. The configuration of electrons and nuclei that results in the lowest energy is known as the ground state. According to the Hohenberg and Kohn theorem, this ground state energy is a unique functional of the electron density. A functional is a mathematical operation that when given a function as an input, gives a number as the output. Therefore the electron density, which is a probability function that describes the location of an electron, can be used to determine the ground state energy. The second theorem by Hohenberg and Kohn showed that the electron density that minimizes the overall energy of the functional is the true electron density, corresponding to the full solution of Schrödinger's equation. For each electron density, there exists a corresponding energy value. If the exact form of the functional used to determine the energy were known, the electron density which results in the lowest energy value would be the true electron density (Sholl et al., 2011).

The exact form of the functional described by the Hohenberg-Kohn theorem is unknown, but the Kohn-Sham equations allow for an approximation of this functional in terms of a single electron, shown in equation [4].

$$\left[\frac{-h^2}{m}\nabla^2 + V(r) + V_H(r) + V_{XC}(r)\right]\Psi_i(r) = \varepsilon_i\Psi_i(r) \quad [4]$$

The terms described in the functional above from left to right are the kinetic energy of the electrons, the potential of the interaction between electrons and the nuclei, the Hartree potential which defines the electron-electron interactions, and the exchange-correlation potential. The

exchange-correlation potential is an unknown contribution that functions as a correction factor to account for effects that are ignored in defining the other terms of the functional and therefore must be approximated. Many approximations are available to define the exchange-correlation. One of the simplest and most common exchange-correlation functionals is the local density approximation (LDA). As the name suggests, the LDA approximation uses the local electron density, or the probability of finding an electron in a specific area, to define the approximate exchange-correlation functional. Another popular approximation used to define the exchange-correlation functional is the generalized gradient approximation (GGA). The GGA approximation uses information about local electron density and the local gradient in the electron density to define the exchange-correlation functional. The local gradient can be incorporated into the GGA functional in various ways, and thus gives rise to many different GGA functionals. The most common are Perdew-Wang functional (PW91) and Perdew-Burke-Ernzerhof functional (PBE) (Sholl et al., 2011).

Though the DFT model is a popular approach for finding solutions to the Schrödinger equation, there are some well-known inaccuracies, such as the underestimation of calculated band gaps in semiconducting and insulating materials. Despite this inaccuracy, the DFT model remains a popular approach due to a multitude of reasons. It is relatively simple, applicable to a wide range of materials, and is generally reliable (Giustino, 2014). It is for these reasons that we used the DFT model in calculations involving MXenes.

DFT calculations are often used in the analysis of the electronic properties of MXenes due to their relatively high reliability and low computational power requirements. These calculations can range from predicting the stability of different MXene arrangements (Anasori et. al, 2015) to exploring the use of MXene quantum dots as an electrocatalyst (Kong et al., 2021). In general, computational software is required to perform DFT calculations. A common software used is the Vienna Ab Initio Simulation Package (VASP) (“The VASP manual”, n.d). In using this package, the k-point values must be specified. The k-point values describe certain points in the Brillouin zone, which is located in reciprocal space. The space represents the Fourier transform of the direct lattice, and certain properties of the material can be related to the Brillouin zone which allows for the understanding of electronic energy bands. Moreover, choosing, or sampling, an appropriate number of k-point values is necessary for an accurate simulation. Ultimately, the understanding of these electron energy bands is important to the electronic properties of the material, as the bands describe the behavior of electrons within the material, which is the basis of the material’s electronic properties. For example, the presence of a band gap would indicate the material is an insulator or semiconductor while the absence of a band gap indicates it would be a metal. In general, it can be seen that DFT provides a relatively simple and reliable way to simulate the structure of MXenes and predict their properties.

3.0 Methodology

In this project, different MXenes with the formula $M_3C_2T_2$ were modeled and visualized using VESTA (see Figure 7), where T represents a termination group which in this case was F, O, and OH. This was done in an effort to determine the different physical, chemical, and electronic properties of the MXenes. These different properties were determined by performing different calculations such as calculating the band structure, work function, and lattice parameter optimization. The main tool used to perform these calculations was DFT.

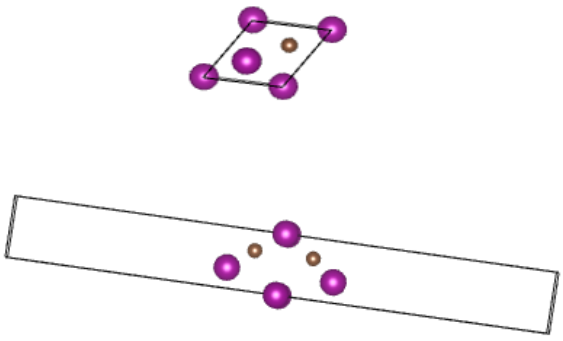

Figure 7: Top (top) and side (bottom) view of the triclinic unit cell of Mn_3C_2 modeled using VESTA software where the purple dots represent the Mn atoms and the brown dots represent C atoms. The model represents a 1x1 cell with a vacuum space of 18.03562 Å.

DFT calculations were performed with the Vienna Ab initio simulation package (VASP) based on the Kohn−Sham density functional theory (Kresse and Furthmüller, 1996). The electron-nuclei interactions were described using the projector augmented wave (PAW) potentials (Kresse and Joubert, 1999)— recommended by VaspWiki—and the exchange-correlation was accounted for using generalized gradient approximation (GGA) by Perdew−Burke−Ernzerhof (PBE) (Perdew et al., 1996). During relaxation, the convergence of total energies and forces was specified to 0.01 meV and -0.01 eV/Å, respectively, using a wave cutoff energy of 450 eV. A gamma-centered 8x8x1 Monkhorst−Pack k-point grid was used. A sigma value of 0.04 eV was used for all calculations except for the density of states. For the density of states, sigma was chosen to be 0.25 eV, as this value gave plots with little noise in the data. For structure optimization, tetrahedron smearing was used. Gaussian smearing was used for the density of states (DOS) and band structure calculations. All of the above parameters mentioned—k-point grid, EDIFF, EDIFFG, wave cutoff energy, and ISMEAR—except for sigma, were optimized by Emily Sutherland, a Ph.D. student at WPI, by increasing the value until it did not change the results significantly. POSCAR files were generated from structure files downloaded from the Computational 2D Materials Database (C2DB) (Haastrup et al., 2018) (Gjerding et al., 2021). The vacuum spaces recommended by C2DB were used for each MXene, which differed between each but overall was around 20 Å. The POSCAR files were exported to fractional coordinates using VESTA (Momma and Izumi, 2011). Vaspkit was utilized for band structure and density of states calculations (Wang et al., 2021). See Appendix 1 for sample input files used in the calculations.

4.0 Results and Analysis

This section will present our results based on the methodology detailed in the previous section. We performed lattice parameter and functional group optimization calculations which also provided us with the magnetic moment for each MXene. We also calculated the total and projected/partial density of states, band structure, and work function of each MXene which provided us with information on which of the MXenes modeled could be useful in photocatalysis. We compared our results to those that were available in the C2DB database and noted any trends in the data.

4.1 Lattice Parameter and Functional Group Optimization

Lattice parameters represent the physical dimensions of the unit cell which make up the MXene lattice. In this project, a total of forty-eight MXenes were modeled. The optimized lattice parameters were calculated using coordinate data from C2DB and input parameters optimized by a graduate student researcher. The files were then inputted into VASP which generated lattice constant energy values for the range of lattice parameters. The lattice parameter which gave the lowest energy value was taken as the optimized lattice parameter. The resulting lattice constants can be seen in Figure 8. In assessing the validity of these results, the lattice parameters obtained were compared to C2DB as shown in Figure 9. This figure shows that the lattice parameter values obtained were in accordance with those in C2DB.

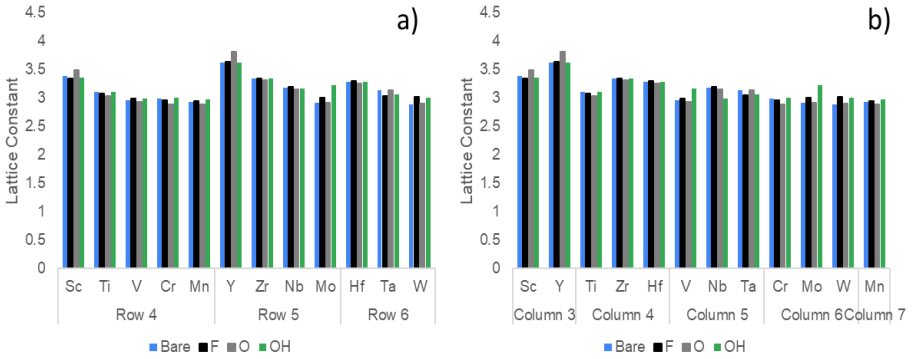

Figure 8: Lattice parameters for different MXenes arranged according to row number (a) and column number (b).

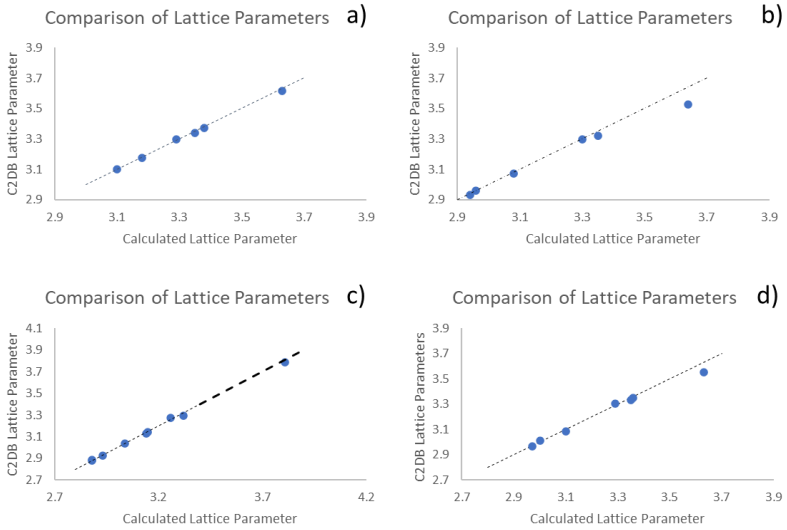

Figure 9: Comparison between our calculated lattice parameters and results from the Computational 2D Materials Database for bare (a), F terminated (b), O terminated (c), and OH terminated (d) MXenes.

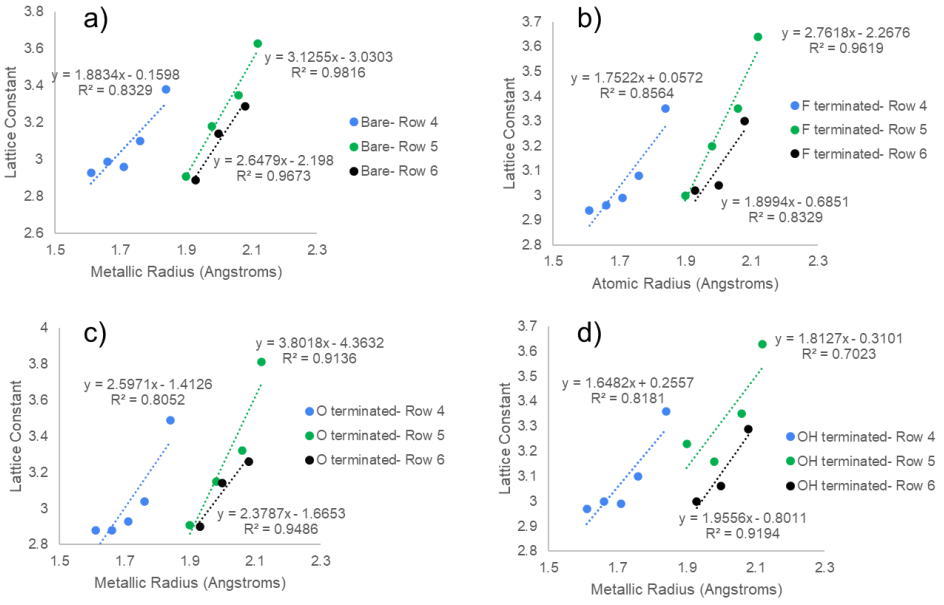

Figure 10: Plot of the relationship between atomic radii (Elements, atomic radii and the periodic table n.d.) and the MXene lattice parameter for bare (a), F terminated (b), O terminated (c), and OH terminated (d) MXenes.

Various trends occur when looking at the lattice parameter values. As shown in Figure 8a, across the rows, the transition metal with the lower atomic number has a larger lattice parameter, with the exception of Row 5 where $Mo_3C_2O_2H_2$ has a larger lattice parameter than $Nb_3C_2O_2H_2$. The decrease in lattice parameters across the row can be attributed to the decrease in the radius of the transition metal within the MXene (see Figure 10). Generally, in a given row, as the size of the transition metal decreases, the unit cell volume and therefore the lattice parameters also decrease. The correlation between the size of the transition metal and the lattice parameter is also noted when looking at Figure 8b. Here, one can see that the lattice constant generally increases down the group, with the exception of the OH terminated MXenes in group three, which corresponds to the increase in the size of the transition metal as one progresses down a group. It should be noted, however, that the differences between the lattice parameters of the latter elements within a group are much smaller than that between the first element and the other elements of the group, with the exception of group four transition metals. A similar trend is also noted by Luo et al (2020) where they describe the fourth period elements (smallest atomic number) within the same group as having a smaller lattice parameter, while the fifth and sixth row elements have similar lattice constants. They attribute this smaller variation in lattice parameter size between the fifth and sixth row elements to a similarity in electronegativity.

Trends also emerge when looking at the different termination groups for the MXenes. In general, O terminated MXenes have a smaller lattice parameter, while OH terminated MXenes have a larger lattice parameter. The smaller lattice parameter exhibited by O terminated MXenes may be attributed to the presence of a covalent bond between the oxygen termination and the rest of the MXene. Covalent bonds are typically shorter and stronger, therefore, resulting in a more compact structure and ultimately a smaller lattice parameter. The larger lattice constant exhibited by OH terminated MXenes when compared to F terminated MXenes may be a result of a difference in electronegativity. As O is less electronegative than F, the resulting bond between OH and the rest of the MXene may be weaker when compared to F and the rest of the MXene. This weaker bond may result in a less compact structure and ultimately a larger lattice parameter. The overall comparison between lattice parameters obtained in this project and by Luo et al

(2020) can be seen in Figure 11. Figure 11 showed more variation in results when compared to Figure 9.

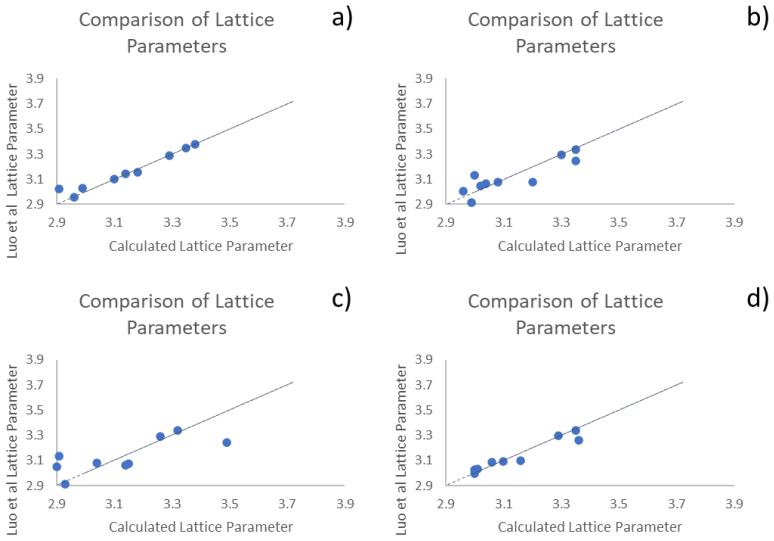

Figure 11: Comparison between lattice parameters results in this project and Luo et al (2020) for bare (a), F terminated (b), O terminated (c), and OH terminated (d) MXenes.

We also utilized lattice parameters to determine the most stable configuration of the MXenes. There are three possible configurations for terminated MXenes: Type I, Type II, and Type III which are shown in Figure 12. In Type I configurations, the termination groups are above the second closest metal layer, in Type II the termination groups are located above the closest X layer (carbon in this project), and Type III configurations have a Type I configuration on the top and a Type II configuration on the bottom, or vice versa. In determining the optimized lattice parameter, all three configurations for the terminated MXenes were modeled.

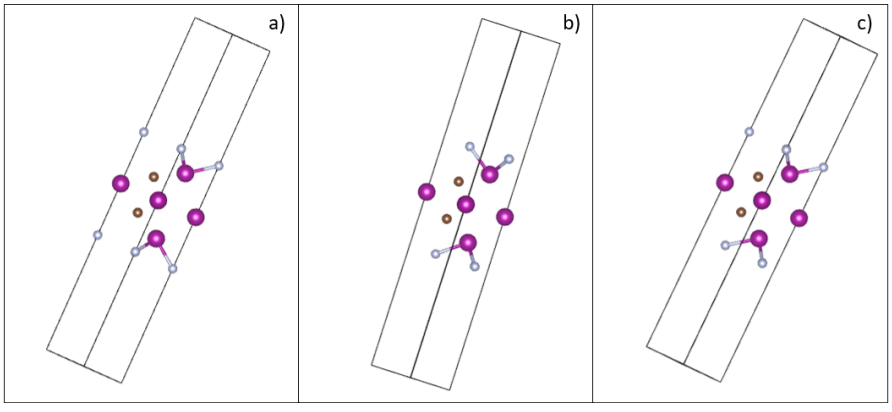

Figure 12: Type I (a), Type II (b), and Type III (c) configurations of $Mn_3C_2F_2$ modeled using VESTA software where the purple dots represent the Mn atoms, the brown dots represent C atoms, and the light blue dots represent F atoms.

Of the thirty-six terminated MXenes modeled, twenty-eight had Type I configuration as their most stable and eight had Type II as their most stable. No MXenes exhibited Type III configuration as its most stable form. When analyzing the MXenes that displayed the different configurations, it was noted that some transition elements displayed the same configuration irrespective of the termination group, while others changed configuration with a change in the termination group, as shown in Figure 13. Tantalum (Ta), the only metal to display multiple configurations, exhibited Type I configuration for the O terminated MXene and Type II for the other terminations. The results of our calculations varied from the work done by other

researchers such as Luo et al (2020) whose findings showed F and OH terminations of Vanadium (V), Niobium (Nb), and Ta to have Type two configurations while F terminated Molybdenum (Mo) and Tungsten (W) had a configuration which was not studied in this work. We used an 8x8x1 k-point mesh to determine the lattice parameter, whereas Luo et al used a 12x12x1 k-point mesh.

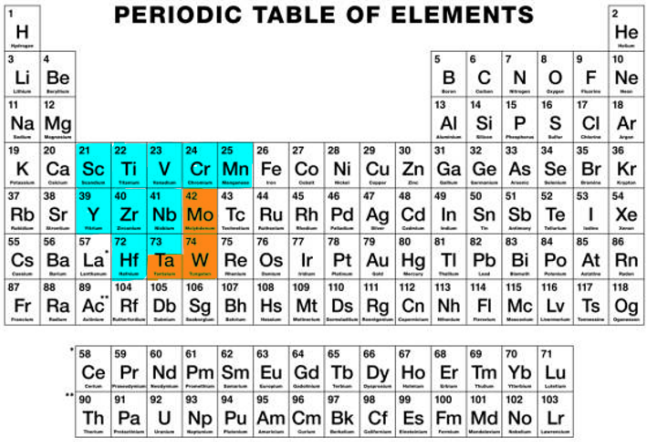

Figure 13: Transition metals that exhibited Type I configurations (highlighted in blue), Type II configurations (highlighted in orange), and multiple configurations (highlighted in blue and orange).

4.2 Magnetic Moment

The magnetic moment refers to the sum of all spins of the electrons in an atom. For instance, if the number of spin-up electrons and the number of spin-down electrons are equal, the net magnetic moment would be zero. If there is one more spin-up electron compared to spin-down electrons, the magnetic moment would be one. The magnetic moment was determined during the lattice optimization process. The optimization process yielded a file over a range of lattice parameter values with a corresponding energy value and magnetic moment. Once the optimized lattice parameter was determined, the corresponding magnetic moment of the most stable structure was used. Generally, Manganese (Mn) and Chromium (Cr) exhibited the highest magnetism (see Figure 14). The high magnetism of Cr and Mn can be attributed to the presence of 3d orbitals. The 3d orbitals weakly overlap producing narrow d-bands which results in magnetic properties. This weak overlap becomes more pronounced as one progresses across the transition metals in the fourth row (Libretexts, 2021).

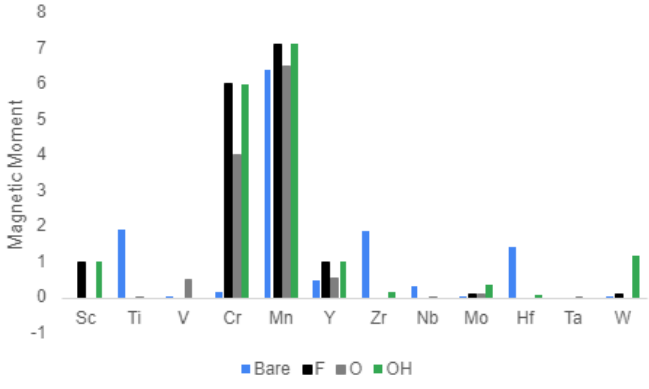

Figure 14: Magnetic moment results for MXenes.

In terms of termination groups, F terminated and OH terminated MXenes generally exhibited the highest magnetic moments. Titanium (Ti), V, Zirconium, Nb, and Hafnium (Hf) did not exhibit this trend. For V, the O terminated MXene had the highest magnetic moment and for

the other elements, the bare MXenes have the highest magnetic moment. Similar to the lattice parameters, our magnetic moment results were compared to C2DB and results reported by Luo et al (2020) (see Figure 15). The results were generally in agreement with the exception of Cr_3C_2. Luo et al reported a significantly higher value for Cr_3C_2 than we calculated. The exact cause of this discrepancy is unknown.

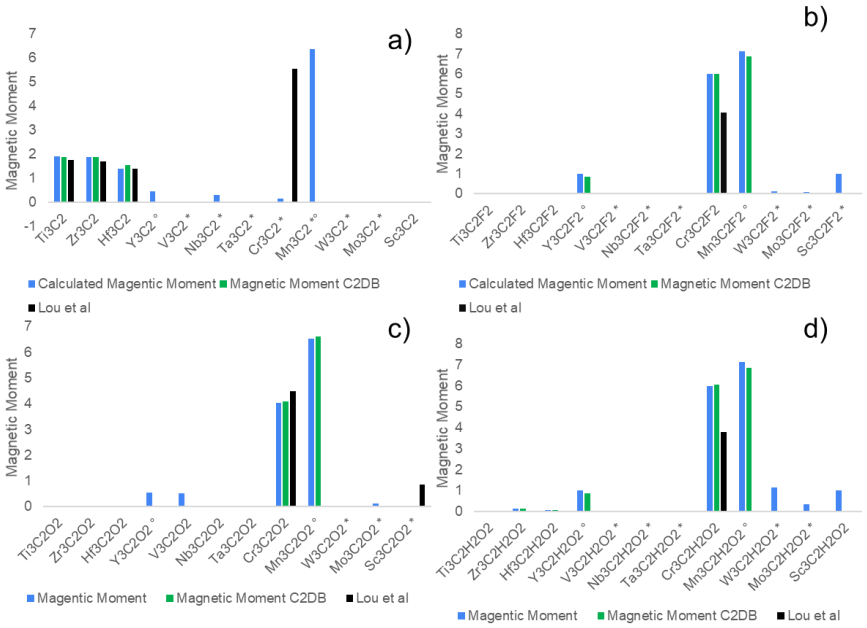

Figure 15: Comparison between magnetic moment results in this project and Luo et al (2020) for bare (a), F terminated (b), O terminated (c), and OH terminated (d) MXenes where * means the MXene was not in C2DB and ° means the MXene was not modeled by Luo et al.

4.3 Density of States

Density of States (DOS) refers to the number of electronic states at an energy level that electrons can occupy (Density of States, 2022). For most MXenes, the density of states near the Fermi level is mostly governed by the transition metal's d-electrons (Hantanasirisakul and Gogotsi, 2018). A higher DOS at the Fermi level—which is a measure of the energy of the least tightly held electrons within a solid—means there are more states available for occupation, which should result in high conductivity of the metal. High conductivity is favorable for photocatalysis because electrons will flow to the surface of the MXene and enhance change carrier separation which increases photocatalytic activity, as discussed in section 2.2, (Brittanica). Insulators, on the other hand, have no electrons at the Fermi level and are not good conductors.

The partial or projected density of states (PDOS) is the relative contribution of each element to the total density of states (TDOS) (Ma et al., 2011). We calculated both TDOS and PDOS for each MXene. Figures 16 and 17 below show our results for terminated MXenes. Each color represents a different element and the key is shown in the left-hand corner. Cr, F, and O contributed the most to the PDOS of the MXenes. Figure 16a below shows the density of states (DOS) for $Cr_3C_2F_2$ from C2DB, rotated so the axis are aligned with our results. Figure 16a-c shows our calculated PDOS and TDOS for $Cr_3C_2F_2$, respectively. Our results are generally similar to C2DB, as the DOS comes to a peak at the Fermi level (see Appendix 2 for a plot of our results as compared to C2DB). Figure 17a shows the C2DB DOS for the OH terminated Cr MXene, and figures 17b-c show our calculated results. Again, this generally matches C2DB, as the DOS has the strongest peak at the Fermi level and decreases on either side. It also shows a peak after -4.

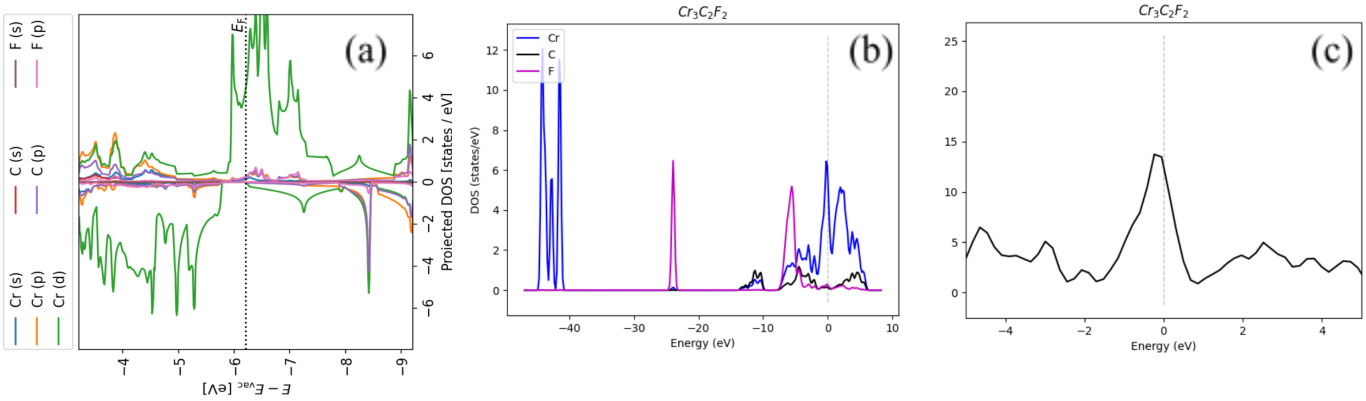

Figure 16: (a) The PDOS of $Cr_3C_2F_2$ from the C2DB database. Each colored line represents the contribution of each element in the MXene to the DOS. As the green line shows, chromium's d electrons contribute the most to the DOS. **(b)** Our calculated PDOS for $Cr_3C_2F_2$. The key is shown in the upper left corner. The dotted grey line represents the Fermi Level, set to 0. **(c)** Our calculated TDOS for $Cr_3C_2F_2$. The DOS is highest at the Fermi level for this MXene, at around 15 states/eV.

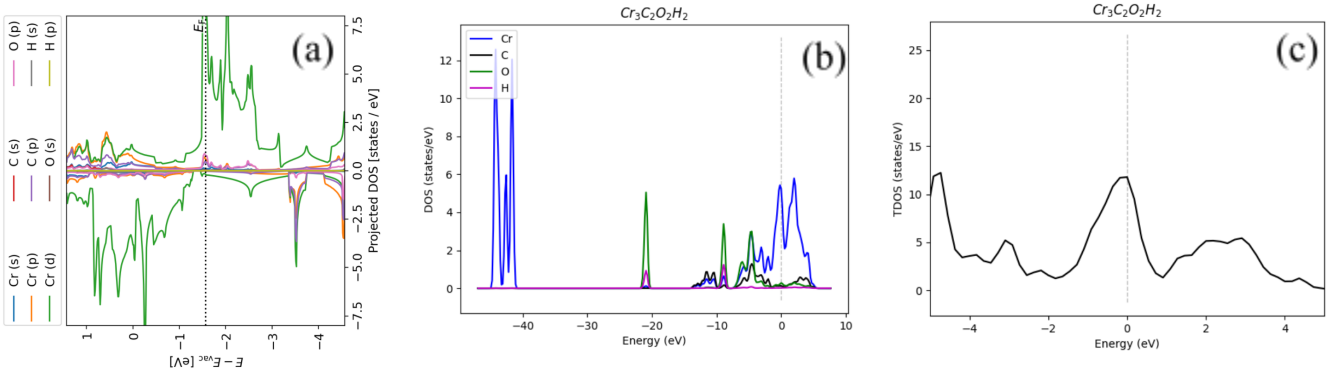

Figure 17: (a) The PDOS for $Cr_3C_2(OH)_2$ from C2DB. Each colored line represents the contribution of each element in the MXene to the DOS. As the green line shows, chromium's d electrons contribute the most to the DOS. **(b)** Our calculated PDOS for $Cr_3C_2(OH)_2$. The key is shown in the upper left corner. The dotted grey line represents the Fermi Level, set to 0. **(c)** Our calculated TDOS for $Cr_3C_2(OH)_2$. The DOS is highest at the Fermi level for this MXene, at around 12 states/eV.

Of the top 10 overall DOS at Fermi level we calculated, 3 were bare MXenes, 3 were OH Terminated, 2 were O terminated, and 2 were F terminated. Bare, F, and OH Terminated Chromium MXenes exhibited especially high DOS at the Fermi level. According to the literature, this is due to Chromium's large magnetic moment due to its half-filled 3d and 4s electron shell (Zhang and Li, 2017). Terminated Y MXenes accounted for 3 of the top 10 DOS, as well as bare and OH terminated V MXenes. A high density of states is favorable for photocatalytic applications because it means there are more states available for electron occupation and therefore result in high conductivity of the metal. See Appendix B for the graph

of all MXenes and their calculated DOS, as well as a scatter plot of our calculated DOS compared to C2DB.

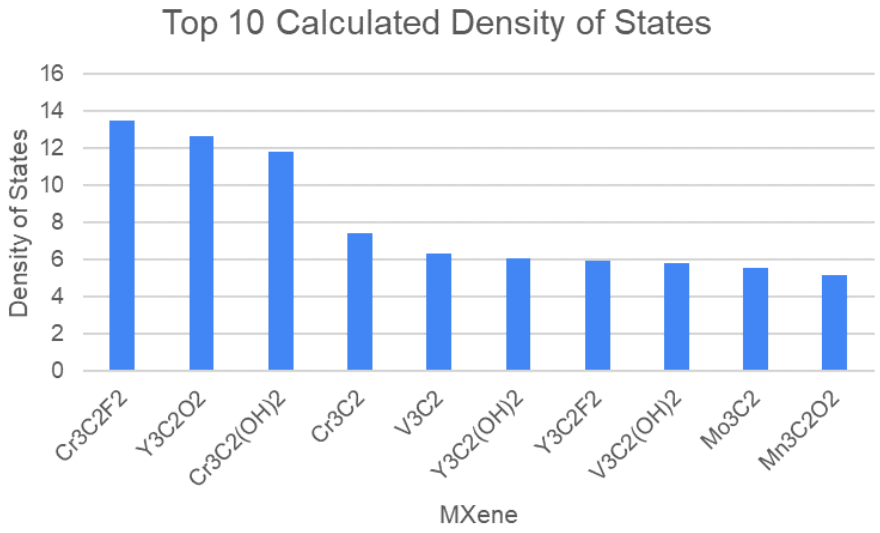

Figure 18: MXenes with the 10 highest calculated density of states at the Fermi level. Chromium (Cr) and Yttrium (Y) each accounted for 3 of the highest DOS, meaning they have many states available for occupation and therefore have good conductivity.

As for trends observed, we found that the density of states generally decreased down a column/group. The density of states increased across a row for Hf, Ta, W for OH terminated, F terminated, and bare MXenes, as can be seen in Figure 19 below. Overall, the DOS of F terminated MXenes was generally lower than the bare, O, and OH terminations, but it was especially lower than O and OH. See appendix B for separate plots of DOS for each termination.

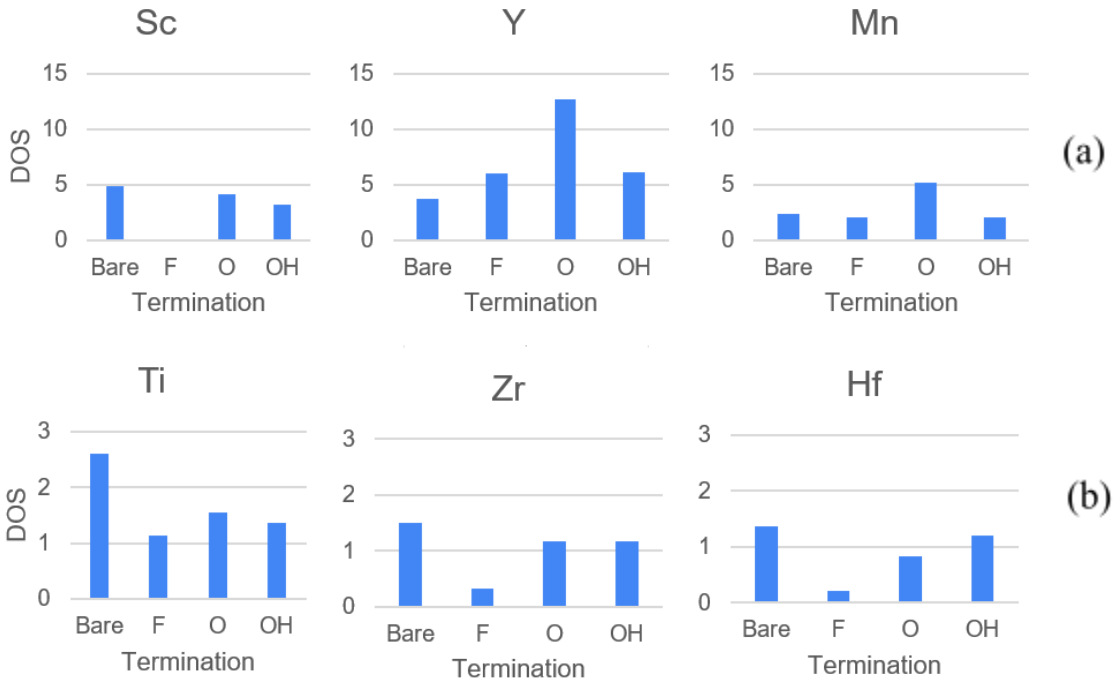

Figure 19 (a-b): Comparison of DOS at the Fermi level for terminations down a group (with the exception of Mn which was the only MXene in its group). Each row (from left to right) represents a group on the periodic table.

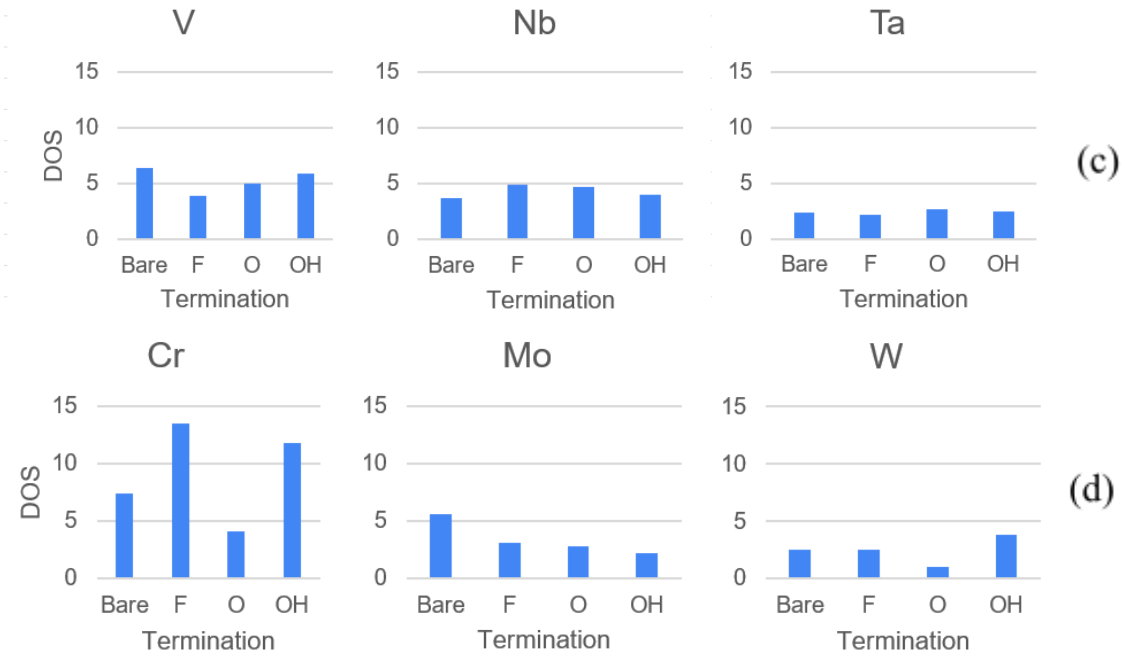

Figure 19 (c-d): Comparison of DOS at the Fermi level for terminations down a group (with the exception of Mn which was the only MXene in its group). Each row (from left to right) represents a group on the periodic table.

As figure 19 shows, for Y, Mn, Nb, Ta, Cr, W, terminations provided a higher DOS, while the rest of the elements had a higher DOS for the bare MXene than any terminations. Bare DOS is typically higher because termination causes new bands to form below the Fermi level, and the Fermi level shifts lower. This leads to lower DOS at the Fermi level due to electron transfer from the transition metal to electronegative surface termination (Hantanasirisakul and Gogotsi, 2018). It is important to note that as figure 20a shows, the DOS for $Sc_3C_2F_2$ was found to be zero which would suggest it is a semiconductor, as its band structure (discussed in section 4.4) also exhibits a small band gap. The rest of the MXenes modeled are metals.

4.4 Band Structure

The band structure of each MXene was analyzed to determine if any band gaps were present. A band gap indicates that the MXene would behave like a semiconductor, while the lack of a band gap indicates the MXene would act like a metal. In figure 20, the three types of band structures are shown. A conductor or metal is when there is no band gap present and electrons can move freely. A semiconductor has a small band gap that still allows for electron transfer, and an insulator has a band gap large enough to prevent any transfer of electrons.

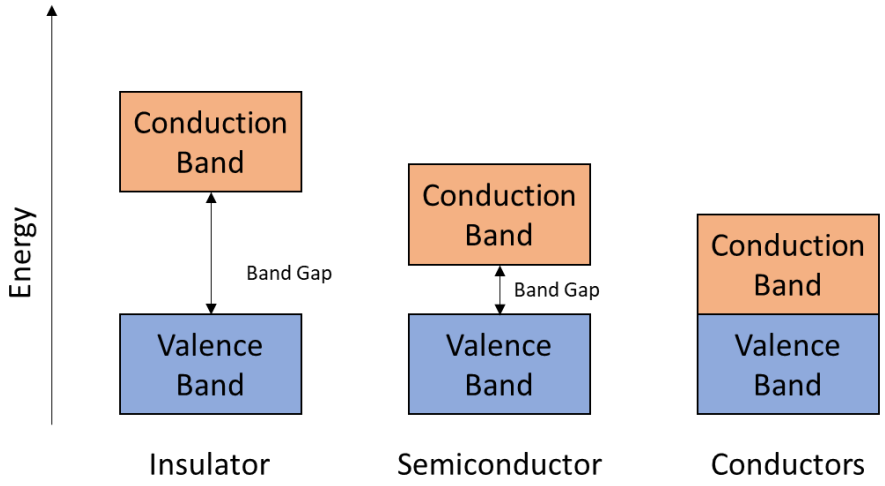

Figure 20: Band Structure from left to right of, Insulator, Semiconductor, and Conductor

Figure 21 shows the band structure of $Sc_3C_2F_2$ which is the only MXene modeled that exhibited a band gap and therefore is a semiconductor. Many of the OH terminated MXenes have a large area of unoccupied space as shown in figure 22. Out of the MXenes we modeled, we expect all of them to behave as metals except for $Sc_3C_2F_2$. None were insulators.

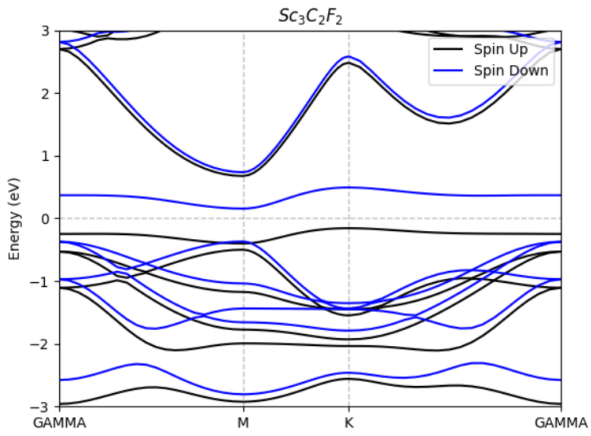

Figure 21: Band Structure of MXene $Sc_3C_2F_2$ which exhibits a band gap.

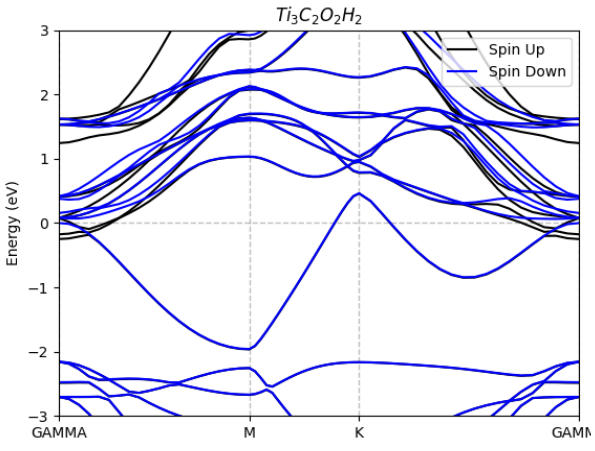

Figure 22: Band Structure of MXene $Ti_3C_2(OH)_2$ there is no clear band gap present, although there is a large unoccupied space.

4.5 Work Function

The work function is the minimum amount of work required to emit one electron from a solid point to a vacuum immediately outside the surface (Kittel, 1996) It is often used as a reference to align the electron levels between different materials. For instance, if the work function is higher in energy for material one compared to material two, then the electrons will spontaneously move from material two to material one because material one's energy levels are lower in energy compared to material two's energy levels, shown in figure 23. Therefore, we want to look for MXenes with high work function values so less energy is required to emit electrons from the semiconductor to the MXene. The work function for each MXene was calculated by finding the difference between the vacuum and Fermi level, as seen in Figure 24.

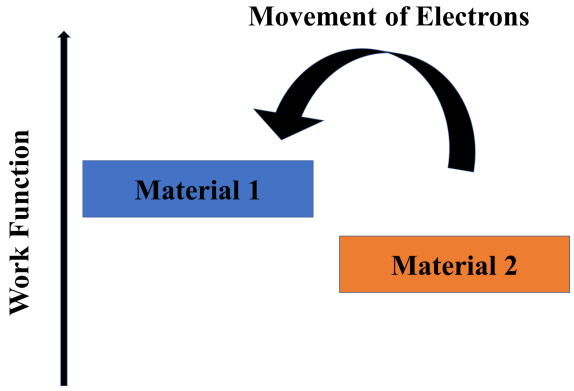

Figure 23: Movement of electrons between two materials with different work functions.

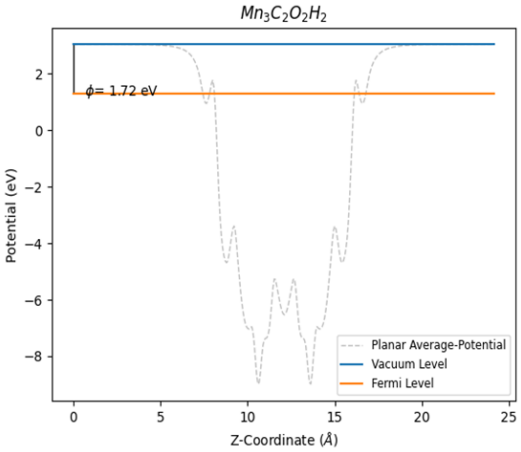

Figure 24: Work Function of MXene $Mn_3C_2(OH)_2$ determined by the difference between Vacuum and Fermi Levels.

After the work function was calculated for each MXene, the values were then compared to the work function values found in the C2DB database (when available). The work function values calculated were generally in agreement with the values found on the database. It should be noted that, on average, there was a greater difference between the calculated and C2DB values for the Bare terminated MXenes than for the other termination groups. The average work function differences for the Bare, F, O, and OH terminations were found to be; 0.368 eV, 0.0518 eV, 0.055 eV, and 0.107 eV respectively. From this, it can be seen that the O terminated MXenes had calculated values that were the closest to the values found in the database.

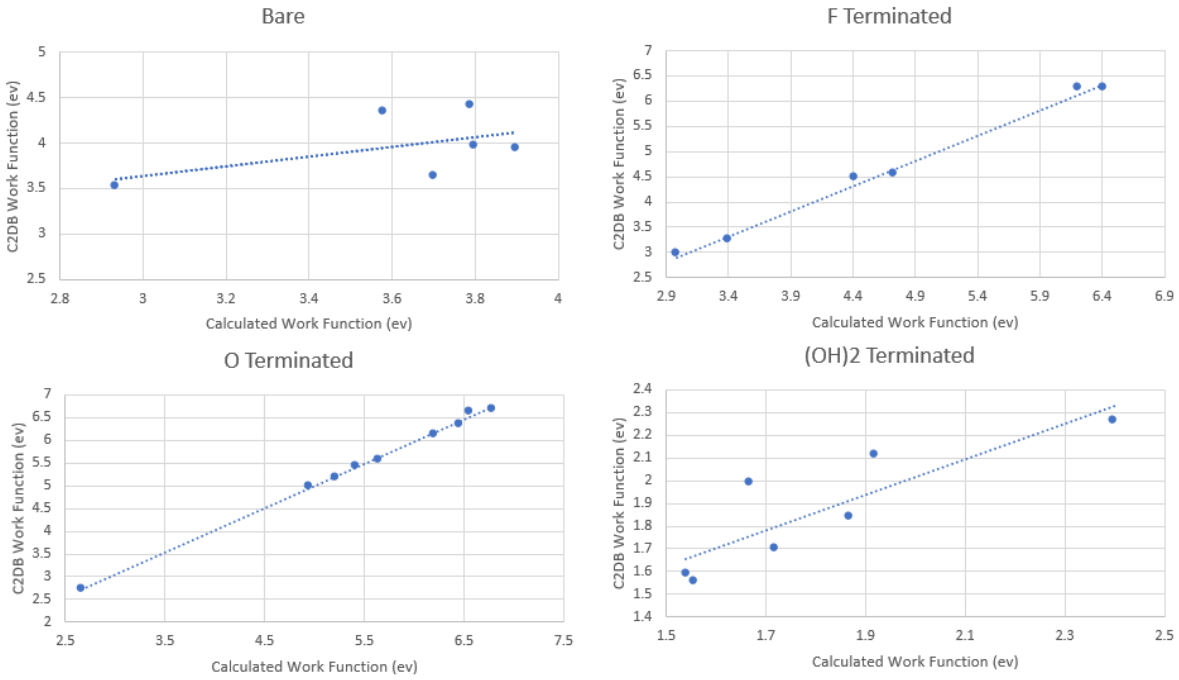

Figure 25: Comparison of calculated MXene work function values with those found in the C2DB database.

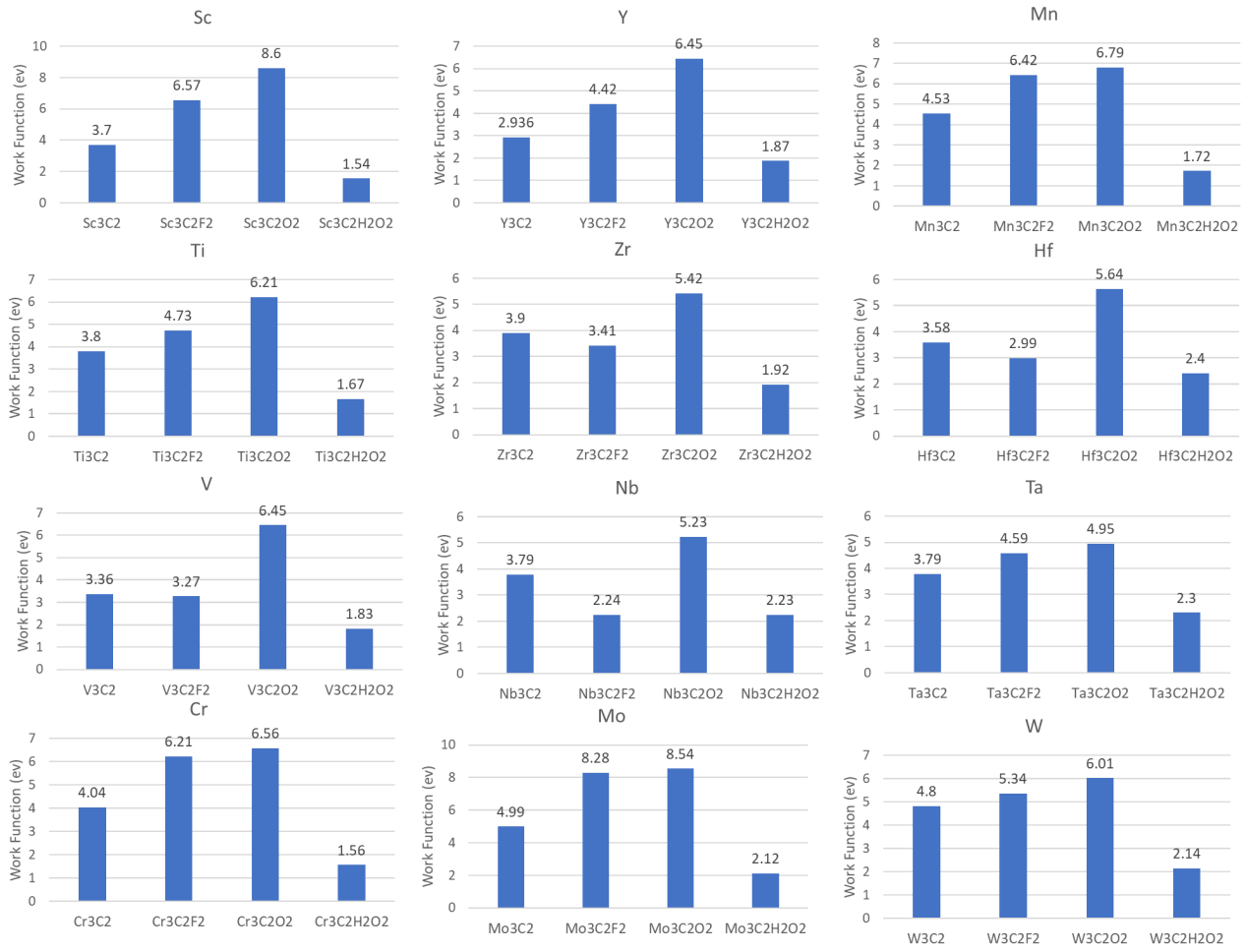

Figure 26: Work function values for MXene terminations down a group (with the exception of Mn which was the only MXene in its group). Each row (from left to right) represents a group on the periodic table.

Figures 25 and 26 above display the work functions of each MXene we calculated, further separated by the termination group, and from this several trends can be identified. The general order of the work functions by termination groups from least to greatest is OH, Bare, F, and O terminated. This trend is present in the majority of the MXenes but not all. The transition metals where this trend is not present are Zr, Hf, V, and Nb. In the case of these MXenes, the Bare termination was greater than the F terminated. However, in all cases, the OH terminated MXenes had the lowest work function value, often by a factor of two to three times. $Sc_3C_2(OH)_2$ had the overall lowest work function value of 1.54 ev and $Hf_3C_2O_2$ had the largest value of 8.6 eV.

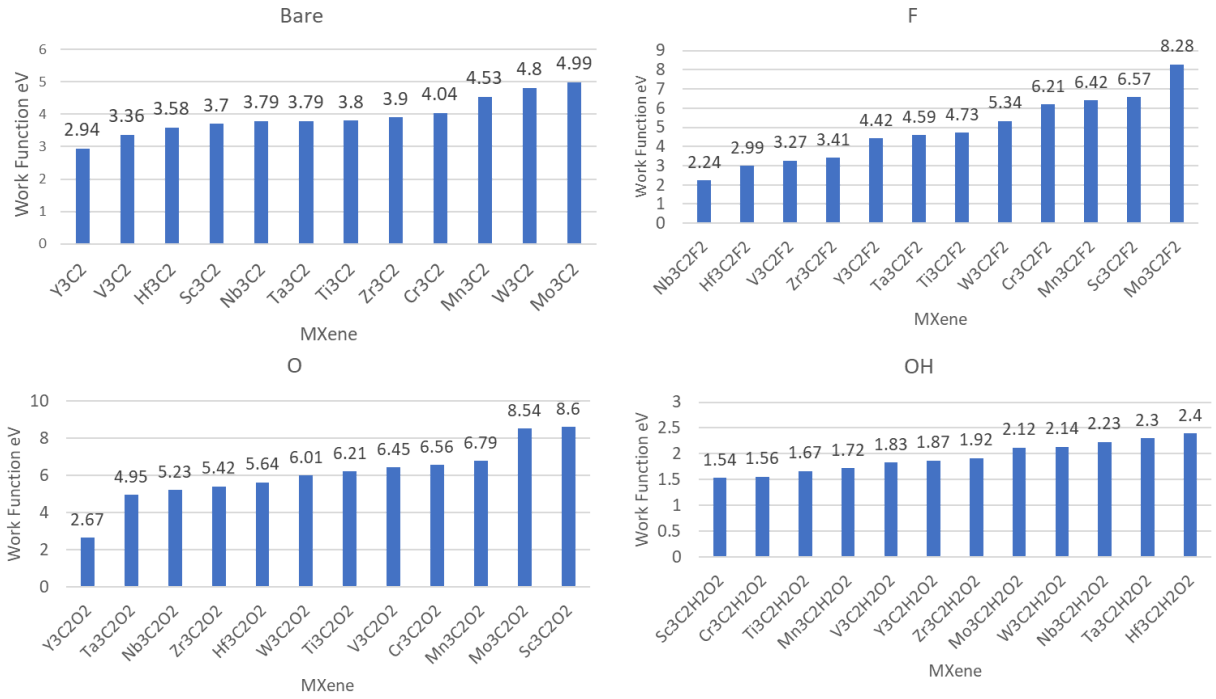

Figure 27: Calculated work function values of MXenes separated by termination group.

Figure 27 shows the same work function values as in Figure 26 but each graph shows one set of termination groups arranged in increasing order. From this, we can see that no MXene has the highest or lowest work function value across all four termination groups. However, it should be noted that transition metals with higher work function values tend to have consistently higher values across termination groups, such as Mo which is in the top half of the work functions in all four terminations. The MXenes with these generally higher work function values are those with transition metals lower in their respective column. This is not a rule but a general trend, and there are exceptions.

Hydrogenated silicon (Si:H) is a common material used as a semiconductor in solar panels, and is the material the work function results will be compared against. The work function value of Si:H can vary between 3.90 and 4.47 eV (Aliani). Recall that electrons move in the direction of low work function to high work function, and so MXenes with a work function value higher than that of Si:H are preferred for use in solar applications. Using the upper range of Si:H's possible work function values of 4.47 eV removes many of the MXenes we looked at from consideration, as all the $(OH)_2$, some of the F, and most of the Bare terminated MXenes have work function values that fall below the threshold. All of the O terminated MXenes except for $Y_3C_2O_2$ have work function values that are greater than 4.47 eV. Of the Bare terminated MXenes only Mn_3C_2, W_3C_2, and Mo_3C_2 have work function values greater than 4.47 eV. Finally about half of the F terminated MXenes, $Ta_3C_2F_2$, $Ti_3C_2F_2$, $W_3C_2F_2$, $Cr_3C_2F_2$, $Mn_3C_2F_2$, $Sc_3C_2F_2$, and $Mo_3C_2F_2$ have work function values higher than Si:H.

5.0 Recommendations and Conclusions

There are several key takeaways about the structure and electromagnetic properties of the MXenes modeled that allow for the recommendation of specific MXenes for use in photocatalytic applications. When it comes to the group of MXenes modeled $M_2C_2T_2$, twenty-eight of thirty-six were type I terminated, while the remaining 8 were type II terminated. This leads to the statement that generally type I is the most stable MXene configuration, although other MXenes such as Nitrogen based MXenes or MXenes with different stoichiometry should be analyzed before generalizing this statement further. None of the MXenes modeled featured a band gap in their band structure apart from $Sc_3C_2F_2$, which is ideal for fast charge transport. However, it should be noted that the band structure of several OH terminated MXenes were close to having band gaps, so it would not be surprising if these MXenes did behave like semiconductors.

The other two properties that are very important when considering materials for use in photocatalysis are their work function value and density of states at the Fermi level. A high density of states is favorable, as a higher density of state near the fermi level implies that there are more states available for electron occupation which in turn means the MXene could be more conductive. The MXenes with the highest density of state values were those with, Cr, Y, or V transition metals. Cr MXenes are of special note because they featured a high magnetic moment. However, across the board, F terminated MXenes had a lower density of states and may not have the fastest charge transport. A work function value higher than 4.47 eV, the work function value corresponding to hydrogenated silicon (Si:H), is desired as Si:H is a common semiconducting material in solar panels. Many MXenes had a work function value larger than 4.47 eV, however the O and F terminated MXenes are of especial note as the higher work function MXenes in these termination groups (Sc, Mo, Mn and Cr) had work functions values upwards of 3.0 eV larger than Si:H. When a MXene is in contact with a semiconductor, electrons will flow from the semiconductor to the MXene if the MXene work function is higher. This is desirable for charge carrier separation as discussed in section 2.2.1.

Based on the results gathered $Cr_3C_2F_2$ is recommended for use in photocatalytic applications over the other MXenes modeled. The combination of Cr transition metal MXenes having high magnetic moments as well as a high density of states, the F termination of Cr having a high work function is what led to this conclusion. An alternative MXene that may be recommended is $V_3C_2O_2$ as it also has a fairly high density of state and work function value, although notably it lacks a strong magnetic moment. $Sc_3C_2F_2$ was the only MXene modeled to exhibit semiconductor properties, so this MXene could also be useful for photocatalysis and further analysis of this MXene and calculation of more properties is recommended.

6.0 References

Alhabeb, M.; Maleski, K.; Anasori, B.; Lelyukh, P.; Clark, L.; Sin, S.; Gogotsi, Y. Guidelines for Synthesis and Processing of Two-Dimensional Titanium Carbide (ti3c2tx MXene). *Chemistry of Materials* **2017**, *29* (18), 7633–7644.

Aliani, C., Krichen, M. & Zouari, A. Effect of the front-metal work function on the performance of a-Si:H(n+)/a-Si:H(i)/c-Si(p) heterojunction solar cells. *J Comput Electron* 18, 576–583 (2019). https://doi.org/10.1007/s10825-019-01324-4

Ameta, R.; Solanki, M. S.; Benjamin, S.; Ameta, S. C. Chapter 6 - Photocatalysis. In *Advanced Oxidation Processes for Waste Water Treatment*; Academic Press, 2018; pp 135–175. https://doi.org/10.1016/B978-0-12-810499-6.00006-1

Anasori, B.; Xie, Y.; Beidaghi, M.; Lu, J.; Hosler, B. C.; Hultman, L.; Kent, P. R.; Gogotsi, Y.; Barsoum, M. W. Two-Dimensional, Ordered, Double Transition Metals Carbides (MXenes). *ACS Nano* **2015**, *9* (10), 9507–9516.

Aral, H.; Vecchio-Sadus, A. Toxicity of Lithium to Humans and the Environment—a Literature Review. *Ecotoxicology and Environmental Safety* **2008**, *70* (3), 349–356.

Aslam, M. K.; Niu, Y.; Xu, M. MXenes for Non‐Lithium‐Ion (Na, K, Ca, Mg, and Al) Batteries and Supercapacitors. *Advanced Energy Materials* **2020**, *11* (2), 2000681.

Brillouin Zone. https://dictionary.iucr.org/Brillouin_zone (accessed Dec 17, 2021).

Caffrey, N. M. Effect of Mixed Surface Terminations on the Structural and Electrochemical Properties of Two-Dimensional ti3c2t2 and v2ct2 MXenes Multilayers. *Nanoscale* **2018**, *10* (28), 13520–13530.

Cui, G.; Sun, X.; Zhang, G.; Zhang, Z.; Liu, H.; Gu, J.; Gu, G. Electromagnetic Absorption Performance of Two-Dimensional MXene ti3c2tx Exfoliated by Hcl + Lif Etchant with Diverse Etching Times. *Materials Letters* **2019**, *252*, 8–10.

Cheng, L.; Li, X.; Zhang, H.; Xiang, Q. Two-Dimensional Transition Metal MXene-Based Photocatalysts for Solar Fuel Generation. *The Journal of Physical Chemistry Letters* **2019**, *10* (12), 3488–3494. http://dx.doi.org/10.1021/acs.jpclett.9b00736

Champagne, A.; Charlier, J.-C. Physical Properties of 2D MXENES: From a Theoretical Perspective. *Journal of Physics: Materials* **2020**, *3* (3), 032006.

Computational Chemistry. https://www.chemeurope.com/en/encyclopedia/Computational_chemistry.html (accessed Oct 7, 2021).

Density of States https://eng.libretexts.org/@go/page/312 (accessed Mar 2, 2022).

Elements, atomic radii and the periodic table. Elements, Atomic Radii and the Periodic Radii. (n.d.). Retrieved April 7, 2022, from http://crystalmaker.com/support/tutorials/atomic-radii/index.html

Energy Band Gap Diagram. Electronics Coach. Retrieved April 19, 2022, from

https://electronicscoach.com/material.html/energy-band-gap-diagram.

Fermi level. https://www.britannica.com/science/Fermi-level (accessed Oct 7, 2021).

Giustino, liciano. *Materials modelling using density functional theory: Properties and predictions*; Oxford University Press: Oxford, 2014; pp 1–12.

Gjerding, M. N.; Taghizadeh, A.; Rasmussen, A.; Ali, S.; Bertoldo, F.; Deilmann, T.; Knøsgaard, N. R.; Kruse, M.; Larsen, A. H.; Manti, S.; Pedersen, T. G.; Petralanda, U.; Skovhus, T.; Svendsen, M. K.; Mortensen, J. J.; Olsen, T.; Thygesen, K. S. Recent Progress of the Computational 2D Materials Database (C2DB). *2D Materials* **2021**, *8* (4), 044002.

Gogotsi, Y.; Huang, Q. MXenes: Two-Dimensional Building Blocks for Future Materials and Devices. *ACS Nano* **2021**, *15* (4), 5775–5780.

Gogotsi, Y.; Anasori, B. The Rise of MXenes. *ACS Nano* **2019**, *13* (8), 8491–8494.

Haastrup, S.; Strange, M.; Pandey, M.; Deilmann, T.; Schmidt, P. S.; Hinsche, N. F.; Gjerding, M. N.; Torelli, D.; Larsen, P. M.; Riis-Jensen, A. C.; Gath, J.; Jacobsen, K. W.; Jørgen Mortensen, J.; Olsen, T.; Thygesen, K. S. The Computational 2D Materials Database: High-Throughput Modeling and Discovery of Atomically Thin Crystals. *2D Materials* **2018**, *5* (4), 042002.

Hantanasirisakul, K.; Gogotsi, Y. Electronic and Optical Properties of 2D Transition Metal Carbides and Nitrides (MXenes). *Advanced Materials* **2018**, *30* (52), 1804779. https://doi.org/10.1002/adma.201804779.

Hart, J.L., Hantanasirisakul, K., Lang, A.C. *et al.* Control of MXenes' electronic properties through termination and intercalation. *Nat Commun* 10, 522 (2019). https://doi.org/10.1038/s41467-018-08169-8

https://dictionary.apa.org/empirical-method (accessed Oct 15, 2021).

Huang, W.; Hu, L.; Tang, Y.; Xie, Z.; Zhang, H. Recent Advances in Functional 2D MXene‐Based Nanostructures for next‐Generation Devices. *Advanced Functional Materials* **2020**, *30* (49), 2005223.

Innomind; Musk, E. The first principles method explained by Elon Musk - YouTube. https://www.youtube.com/watch?v=NV3sBlRgzTI (accessed Oct 15, 2021).

Khazaei, M.; Ranjbar, A.; Arai, M.; Sasaki, T.; Yunoki, S. Electronic Properties and Applications of MXenes: A Theoretical Review. *Journal of Materials Chemistry C* **2017**, *5* (10), 2488–2503.

Kittel, Charles (1996). *Introduction to Solid State Physics* (7th ed.). Wiley.

Kong, Q.; An, X.; Huang, L.; Wang, X.; Feng, W.; Qiu, S.; Wang, Q.; Sun, C. A DFT Study of Ti3C2O2 MXenes Quantum Dots Supported on Single Layer Graphene: Electronic Structure an Hydrogen Evolution Performance. *Frontiers of Physics* **2021**, *16* (5).

Kresse, G.; Furthmüller, J. Efficient Iterative Schemes for Ab Initio Total-Energy Calculations Using a Plane-Wave Basis Set. *Physical Review B* **1996**, *54*, 11169. https://doi.org/10.1103/PhysRevB.54.11169.

Kresse, G.; Joubert, D. From Ultrasoft Pseudopotentials to the Projector Augmented-Wave Method. *Phys. Rev. B* **1999**, *59*, 1758-. https://doi.org/10.1103/PhysRevB.59.1758.

Kuang, P.; Low, J.; Cheng, B.; Yu, J.; Fan, J. MXene-Based Photocatalysts. *Journal of Materials Science & Technology* **2020,** *56*; 18–44. https://doi.org/10.1016/j.jmst.2020.02.037

Libretexts. (2021, June 8). *6.7: Atomic orbitals and magnetism*. Chemistry LibreTexts. Retrieved April 12, 2022, from https://chem.libretexts.org/Bookshelves/Inorganic_Chemistry/Book%3A_Introduction_to_Inorganic_Chemistry_(Wikibook)/06%3A_Metals_and_Alloys-_Structure_Bonding_Electronic_and_Magnetic_Properties/6.07%3A_Atomic_Orbitals_and_Magnetism#:~:text=Past%20V%20in%20the%20first,magnetic%20properties%20as%20discussed%20below.

Libretexts. Electron-Hole Recombination. https://eng.libretexts.org/@go/page/323 (accessed Sep 29, 2021).

Li, X.; Wang, C.; Cao, Y.; Wang, G. Functional MXene Materials: Progress of Their Applications. *Chemistry - An Asian Journal* **2018**, *13* (19), 2742–2757.

Li, M.; Lu, J.; Luo, K.; Li, Y.; Chang, K.; Chen, K.; Zhou, J.; Rosen, J.; Hultman, L.; Eklund, P.; Persson, P. O.; Du, S.; Chai, Z.; Huang, Z.; Huang, Q. Element Replacement Approach by Reaction with Lewis Acidic Molten Salts to Synthesize Nanolaminated Max Phases and MXenes. *Journal of the American Chemical Society* **2019**, *141* (11), 4730–4737.

https://www.alibaba.com/product-detail/Research-Grade-Titanium-Carbide-Two-Dimensional_62434625469.html (accessed Jan 31, 2022).

Luo, K., Zha, X. H., Zhou, Y., Huang, Q., Zhou, S., & Du, S. (2020). Theoretical exploration on the vibrational and mechanical properties of M 3 c 2 /M 3 c 2 T 2 mxenes. *International Journal of Quantum Chemistry*, *120*(24). https://doi.org/10.1002/qua.26409

Ma, Z. Y.; Rissner, F.; Wang, L. J.; Heimel, G.; Li, Q. K.; Shuai, Z.; Zojer, E. Electronic Structure of Pyridine-Based Sams on Flat Au(111) Surfaces: Extended Charge Rearrangements and Fermi Level Pinning. *Physical Chemistry Chemical Physics* **2011**, *13* (20), 9747.

Misra, P. K. Basic Properties of Crystals. *Physics of Condensed Matter* **2012**, 1–35.

Mohammad, B. F. (2019). History of the reciprocal lattice. *Powder Diffraction, 34*(3), 260-266. http://dx.doi.org/10.1017/S0885715619000496

Momma, K.; Izumi, F. It VESTA3 for Three-Dimensional Visualization of Crystal, Volumetric and Morphology Data. *Journal of Applied Crystallography* **2011**, *44* (6), 1272–1276. https://doi.org/10.1107/S0021889811038970.

Perdew, J. P.; Burke, K.; Ernzerhof, M. Generalized Gradient Approximation Made Simple. *Physical Review Letters* **1996**, *77* (18), 3865–3868.

Shuck, C. E.; Sarycheva, A.; Anayee, M.; Levitt, A.; Zhu, Y.; Uzun, S.; Balitskiy, V.; Zahorodna, V.; Gogotsi, O.; Gogotsi, Y. Scalable Synthesis of TI 3 c 2 T X MXene. *Advanced Engineering Materials* **2020**, *22* (3), 1901241.

Sholl, D.; Steckel, J. A.; Sholl, D. *Density functional theory: A practical introduction*; Wiley: Somerset, 2011.

VandenBos, G. R. Apa Dictionary of Psychology; American Psychological Association: Washington (D.C.), 2015.

Wang, V.; Xu, N.; Liu, J.-C.; Tang, G.; Geng, W.-T. VASPKIT: A User-Friendly Interface Facilitating High-Throughput Computing and Analysis Using VASP Code. *Computer Physics Communications* **2021**, *267*, 108033.

Webster, N. *The Merriam-Webster Dictionary*; Pocket Books: New York, 1977.

Xin, M.; Li, J.; Ma, Z.; Pan, L.; Shi, Y. MXenes and Their Applications in Wearable Sensors. *Frontiers in Chemistry* **2020**, *8*.

Zhan, X.; Si, C.; Zhou, J.; Sun, Z. MXene and MXene-Based Composites: Synthesis, Properties and Environment-Related Applications. *Nanoscale Horizons* **2020**, *5* (2), 235–258.

Zhang, Y.; Li, F. Robust Half-Metallic Ferromagnetism in Cr3C2 MXene. *Journal of Magnetism and Magnetic Materials* **2017**, *433*, 222–226. https://doi.org/10.1016/j.jmmm.2017.03.031.

7.0 Appendices

APPENDIX 1: Sample Input Files for Lattice Constant Optimization

INCAR

```
SYSTEM=Ti3C2F2

 ENCUT = 450.000000
 SIGMA = 0.040000
 EDIFF = 1.00e-05
 EDIFFG = -1.00e-02
 PREC = accurate
 ISPIN = 2
 ISMEAR = 0
 LREAL = A

 ISTART = 0

 NSW = 300
 IBRION = 2
 ISIF = 2

 LCHARG = .TRUE.
 LWAVE = .TRUE.
 LDAU = .FALSE.
```

KPOINT

```
Ti3C2F2
0
Gamma
8 8 1
0 0 0
```

POSCAR

```
Ti3C2F2:
1.0
      3.0699999332        0.0000000000        0.0000000000
     -1.5350000407        2.6579999754        0.0000000000
      0.0000000000        0.0000000000       22.2409992218
  Ti    C    F
   3    2    2
```

Direct

0.000000000	0.000000000	0.499992788
0.666621387	0.333376348	0.606140435
0.666621387	0.333376348	0.393845320
0.333376348	0.666752696	0.558794677
0.333376348	0.666752696	0.441190839
0.000000000	0.000000000	0.662892878
0.000000000	0.000000000	0.337092638

APPENDIX 2: Additional Density of States Figures

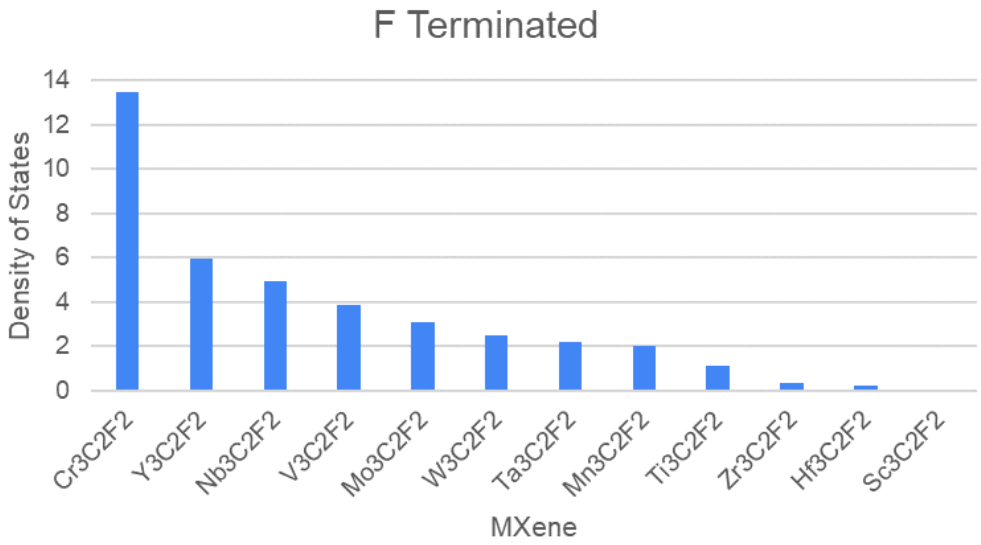

Figure 28: Calculated DOS at Fermi Level for F terminated MXenes.

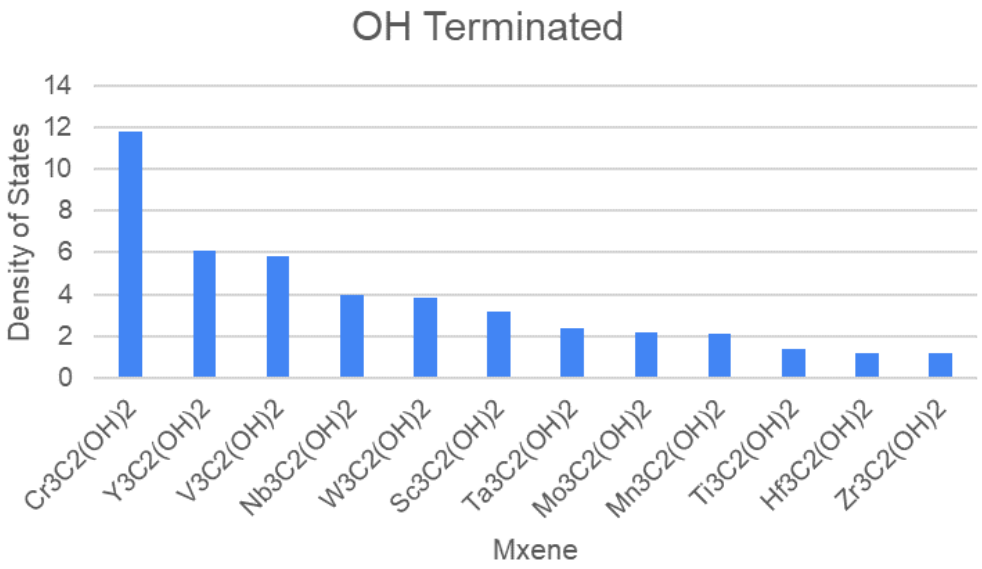

Figure 29: Calculated DOS at Fermi Level for OH terminated MXenes.

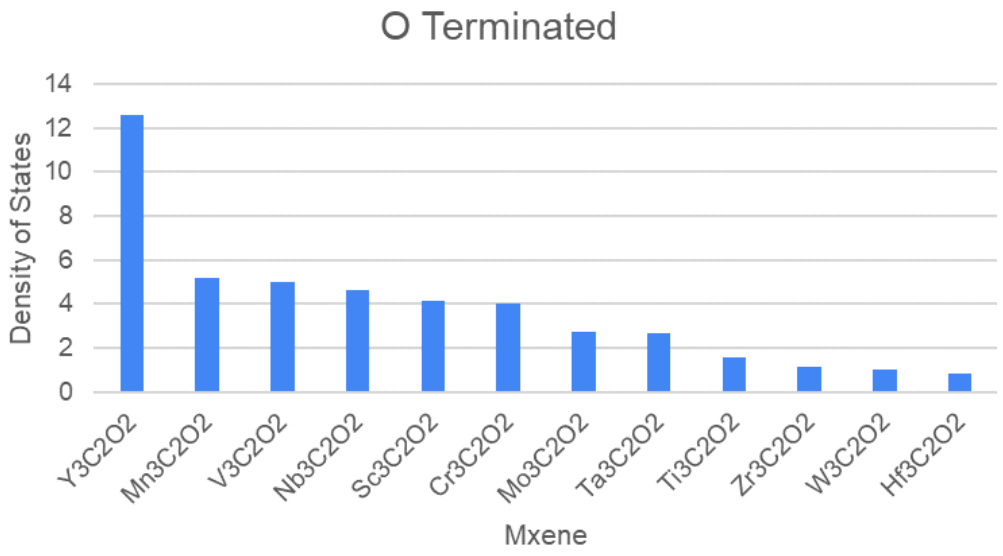

Figure 30: Calculated DOS at Fermi Level for O terminated MXenes.

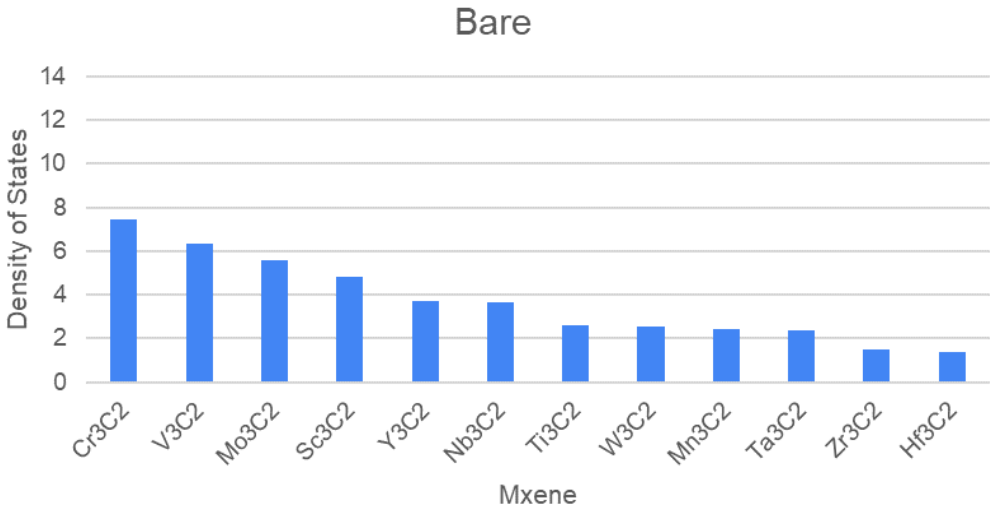

Figure 31: Calculated DOS at Fermi Level for bare MXenes.

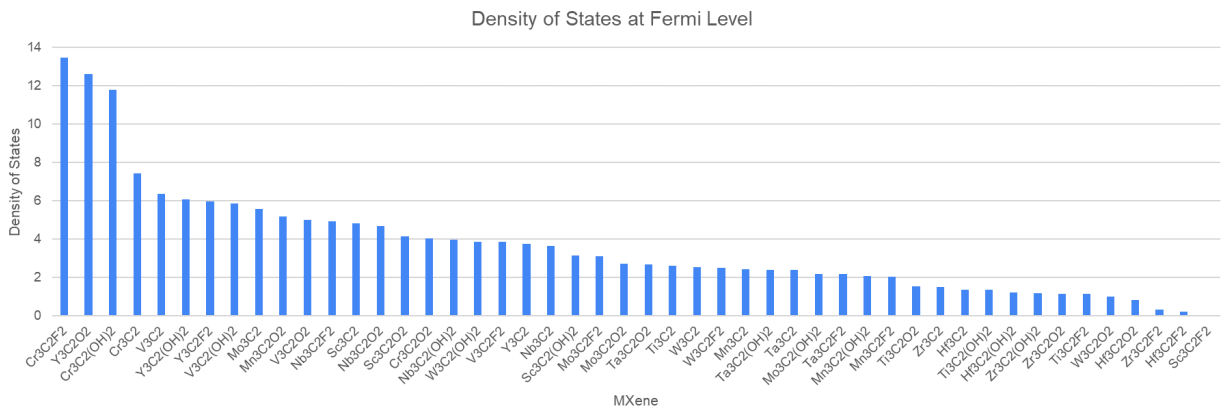

Figure 32: Overall calculated density of states for all MXenes

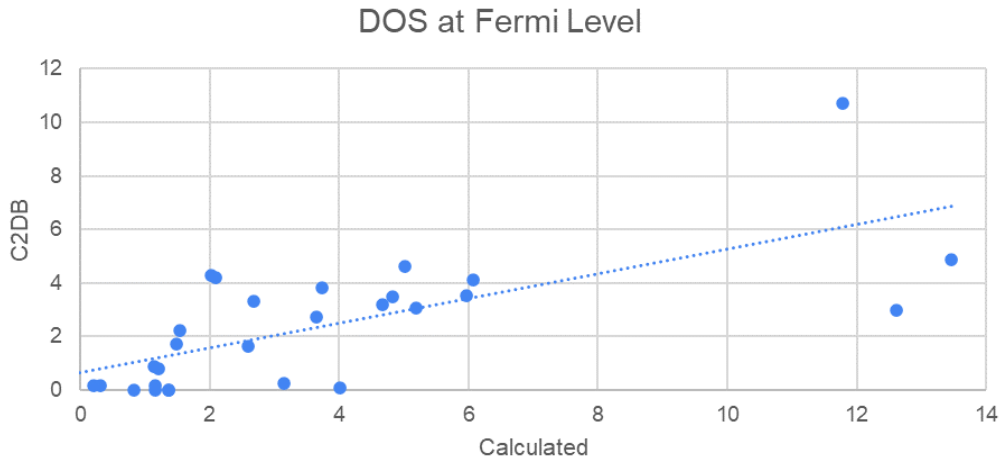

Figure 33: Plot of our calculated DOS at fermi level against the DOS reported by C2DB.